DEVELOPMENT OF A NEW FLAME SPEED VESSEL TO MEASURE THE EFFECT OF STEAM DILUTION ON LAMINAR FLAME SPEEDS OF SYNGAS FUEL BLENDS AT ELEVATED PRESSURES AND TEMPERATURES

A Thesis

by

MICHAEL CHRISTOPHER KREJCI

Submitted to the Office of Graduate Studies of
Texas A&M University
in partial fulfillment of the requirements for the degree of

MASTER OF SCIENCE

May 2012

Major Subject: Mechanical Engineering

Development of a New Flame Speed Vessel to Measure the Effect of Steam Dilution on Laminar Flame Speeds of Syngas Fuel Blends at Elevated Pressures and Temperatures

DEVELOPMENT OF A NEW FLAME SPEED VESSEL TO MEASURE THE EFFECT OF STEAM DILUTION ON LAMINAR FLAME SPEEDS OF SYNGAS FUEL BLENDS AT ELEVATED PRESSURES AND TEMPERATURES

A Thesis

by

MICHAEL CHRISTOPHER KREJCI

Submitted to the Office of Graduate Studies of
Texas A&M University
in partial fulfillment of the requirements for the degree of

MASTER OF SCIENCE

Approved by:

Chair of Committee,	Eric L. Petersen
Committee Members,	Kalyan Annamalai
	Adonios N. Karpetis
Head of Department,	Jerald A. Caton

May 2012

Major Subject: Mechanical Engineering

ABSTRACT

Development of a New Flame Speed Vessel to Measure the Effect of Steam Dilution on Laminar Flame Speeds of Syngas Fuel Blends at Elevated Pressures and Temperatures

(May 2012)

Michael Christopher Krejci, B.S., Texas A&M University

Chair of Advisory Committee: Dr. Eric L. Petersen

Synthetic gas, syngas, is a popular alternative fuel for the gas turbine industry, but the composition of syngas can contain different types and amounts of contaminants, such as carbon dioxide, methane, moisture, and nitrogen, depending on the industrial process involved in its manufacturing. The presence of steam in syngas blends is of particular interest from a thermo-chemical perspective as there is limited information available in the literature. This study investigates the effect of moisture content (0 – 15% by volume), temperature (323 – 423 K), and pressure (1 – 10 atm) on syngas mixtures by measuring the laminar flame speed in a newly developed constant-volume, heated experimental facility. This heated vessel also broadens the experimental field of study in the authors' laboratory to low vapor pressure fuels and other vaporized liquids. The new facility is capable of performing flame speed experiments at an initial pressure as high as 30 atm and an initial temperature up to 600 K. Several validation experiments were performed to demonstrate the complete functionality of the flame speed facility. Additionally, a design-of-experiments methodology was used to study the mentioned syngas conditions that are relevant to the gas turbine industry. The design-of-experiments methodology provided the capability to identify the most influential factor on the laminar flame speed of the conditions studied. The experimental flame speed data are compared to the most up-to-date C4 mechanism developed through collaboration between Texas A&M and the National University of Ireland Galway. Along with good model agreement shown with all presented data, a rigorous uncertainty analysis of the flame speed has been performed showing an extensive range of values from 4.0 cm/s to 16.7 cm/s. The amount of carbon monoxide dilution in the fuel was shown to be the most influential factor on the laminar flame speed from fuel lean to fuel rich. This is

verified by comparing the laminar flame speed of the atmospheric mixtures. Also, the measured Markstein lengths of the atmospheric mixtures are compared and do not demonstrate a strong impact from any one factor but the ratio of hydrogen and carbon monoxide plays a key role. Mixtures with high levels of CO appear to stabilize the flame structure of thermal-diffusive instability. The increase of steam dilution has only a small effect on the laminar flame speed of high-CO mixtures, while more hydrogen-dominated mixtures demonstrate a much larger and negative effect of increasing water content on the laminar flame speed.

ACKNOWLEDGMENTS

First, I would like to greatly thank my advisor, Dr. Eric Petersen, for his tenacious work ethic and availability to his students. His positive attitude inspires his students to perform and achieve the most out of their work. Thanks to Dr. Annamalai and Dr. Karpetis for serving on my committee.

I would also like to thank my former co-worker, Will Lowry, for training me in this field of combustion and providing me the tools to succeed. I also thank my present co-workers, Andrew Vissotski, Sankar Ravi, Drew Plichta, and Travis Sikes, for helping to perform experiments, creating a more efficient overall process, and for continual support and discussion in learning combustion. I thank the rest of my co-workers at the lab for creating a welcoming work place.

Finally, I would like to thank all of those who have been and continue to be a special part of my life. Thank you to my future wife, Ellen, who has stood by my side even when we have not always seen eye to eye. I thank my parents for their guidance throughout my life and for being my financial support all through college. My final thanks go to my brothers and sister who helped develop the person I am now and for their continual support towards my future life.

NOMENCLATURE

Abbreviations

c_p	Specific heat (KJ/kg-K)
$D_{i,j}$	Diffusivity of species *i* into *j* (m^2/s)
h	Specific enthalpy (KJ/kg)
Le	Lewis Number
$\dot{m}"$	Mass burning rate per unit area (kg/m^2-s)
M_w	Molecular weight (kg/kmol)
X	Mole fraction (kmol/kmol)
Y	Mass fraction (kg/kg)

Subscripts

b	Burned condition
i	For species i
L	Laminar flame
u	Unburned condition

Superscripts

o	Un-stretched condition

Greek Symbols

λ	Thermal conductivity (W/m-K)
ρ	Density (kg/m^3)
$S_{L,b}$	Burned, stretched laminar flame speed
$S_{L,b}^o$	Burned, un-stretched laminar flame speed
$S_{L,u}^o$	Unburned, un-stretched laminar flame speed
$\vec{v}$	Velocity (m/s)
$v_{i,diff}$	Diffusion velocity for species *i* (m/s)
$\dot{\omega}_i$	Molar production rate for species *i* (kmol/m^3-s)

TABLE OF CONTENTS

CHAPTER Page

LIST OF FIGURES

Page

Page

Page

Page

LIST OF TABLES

Page

CHAPTER I

INTRODUCTION

The laminar flame speed of premixed combustible mixtures continues to be an important parameter for predicting combustion phenomena, such as flash back, blow off, and dynamic instabilities, and validating chemical kinetic models (Bourque et al., 2008; Lieuwen and Yang, 2005). Several methods have been used to measure the laminar flame speed at high pressures but at standard room temperature such as the outwardly propagating spherical flame, Bunsen burner, counter flow flame, stagnation flame, and heat flux method (Lowry et al., 2011). More recently, some of these methodologies have been upgraded to measure laminar flame speeds at or near- conditions of gas turbine systems, i.e. high pressures, high temperatures, and alternative fuels.

Clean, reliable, and energy-efficient fuels are becoming more important for power systems, such as gas turbines. Many established gas turbines can operate with a wide range of fuels, which makes them an excellent source for clean energy production. Two current major fuel sources that are being developed are hydrogen and synthetic gas, or syngas. Hydrogen's CO_2-free emissions and wide flammability range make it a prime candidate for clean energy; however, hydrogen's fast chemical kinetics and high combustion temperature can prove to be problematic for applications. Syngas can be formed from many processes and feed stocks making it an excellent, reliable energy source, but the composition of syngas can vary greatly depending on the type of feed stock and process. The typical gas composition from various gasifier processes can include 6.8-50.4% H_2, 8.1-60.5% CO, 1.3-29.6% CO_2, 0–20.4% H_2O, 0–9.3% CH_4, and traces of other contaminants (Chacartegui et al., 2011). This variation drives the need to develop and improve chemical kinetic models through experiments with hydrogen and various compositions of syngas at standard and elevated pressures and temperatures. To fully assess the viability of hydrogen and syngas as alternative fuel sources, a detailed understanding of its thermodynamic properties and chemical kinetics

---

This thesis follows the style of *Combustion Science and Technology*.

is required by measuring fundamental parameters, such as laminar flame speed. Several studies have been published on flame speed measurements and analyses of the chemical kinetics effects for both pure hydrogen and syngas compositions.

The chemical kinetics of hydrogen oxidation has been well studied for the past few decades. Therefore, only the most recent studies will be presented related to laminar flame speed and chemical kinetic modeling. Laminar flame speeds of hydrogen and air at standard temperature and pressure have been studied often over a wide range of equivalence ratios (Vagelopoulos et al., 1994; Pareja et al., 2010; Burke et al., 2009). Some laboratories have studied the effects of different diluents at varying ratios of H_2 and O_2 at elevated pressures, up to 60 atm, and standard temperature conditions (Egolfopoulos and Law, 1990; Tse et al., 2000) or at elevated temperatures and atmospheric pressure (Verhelst et al., 2005). More frequently, the initial temperature and pressure are increased together to understand the behavior of laminar flame speeds and how the sensitivity of the sub-reactions change at these conditions (Aung et al., 1997; Dahoe, 2005; Kwon and Faeth, 2001; Hu et al., 2009).

Since the composition of syngas can vary, most researchers change the ratio of hydrogen and carbon monoxide to hopefully gain an understanding of how carbon monoxide affects the hydrogen-oxygen kinetics. There are groups who have strictly studied syngas at standard temperature and pressure (McLean et al., 1994; Dong et al., 2009; Bouvet et al., 2011) while others have additionally varied the pressure, up to 40 atm, at standard temperature (Burke et al., 2007; Hassan et al., 1997; Sun et al., 2007). Contaminants also play a large role in syngas fuel so there have been many efforts to understand the effects of contaminants, such as carbon dioxide (Burke et al., 2010; Natarajan et al., 2005; Lamoureux et al., 2003), steam (Das et al., 2011), and nitrogen (Prathap et al., 2008), on the laminar flame speed and reaction kinetics. Finally, the initial temperature can be varied along with the syngas composition which has demonstrated disagreement with a chemical kinetic model (Natarajan et al., 2005; Natarajan et al., 2009; Kuznetsov et al., 2010).

In order to study hydrogen and syngas compositions at elevated pressures and temperatures, an experimental apparatus must be developed to perform at those elevated conditions and safely contain the combustible mixture. In addition to performing typical combustible, gas mixtures at elevated temperatures and pressure, a high-temperature and high-pressure (HTHP) vessel will also allow the opportunity to study the effects of low vapor pressure fuels, other vaporized liquids (water), and validate chemical kinetic model predictions. After discussing the development of the HTHP vessel, the final objective of this thesis is to investigate the effects of different syngas compositions diluted with varying amounts of water at standard and elevated pressures and temperatures on the laminar flame speed and Markstein length. The Markstein length is a measure of the flame response to stretch. In application systems, the Markstein length is used to calculate the Markstein number, an indicator of the propensity of a system to be influenced by thermo-acoustic instability (Aldredge and Killingsworth, 2004).

This thesis is divided by chapters. In Chapter II, the background of laminar premixed flames is discussed, including the equations that govern a premixed flame. Chapter III covers the development of the HTHP facility used for taking the flame speed measurements in detail, including the design of the vessel, optical system, and validation experiments. Chapter IV details the improved method of data analysis and presents the uncertainty methodology. The Design of Experiment approach and the results are discussed in Chapter V. Chapter VI presents a further discussion of the effect of water dilution on flame speed and how particular reactions are more sensitive in high-carbon monoxide or low-carbon monoxide combustible mixtures. Finally, Chapter VII concludes this thesis.

CHAPTER II

BACKGROUND

The laminar flame speed is a fundamental property to understand the flame-structure and flame-stability characteristics. For several combustion systems, such as gas turbines, the flame speed is important for predicting flash back, blow off, and other dynamic instabilities. Fundamentally, a flame is a self-sustaining propagation of a localized combustion zone at subsonic velocities (Turns, 2000). This defines the flame to occupy only a small portion of the combustible mixture at any one time and must be travelling at subsonic velocities, or exist as a deflagration.

Premixed flames can be described by dividing the flame into two zones, the preheat zone and the reaction zone. Figure 1 shows how the temperature and fuel mass fraction change across the flame thickness, δ, as the reactants enter from the left travelling to the right.

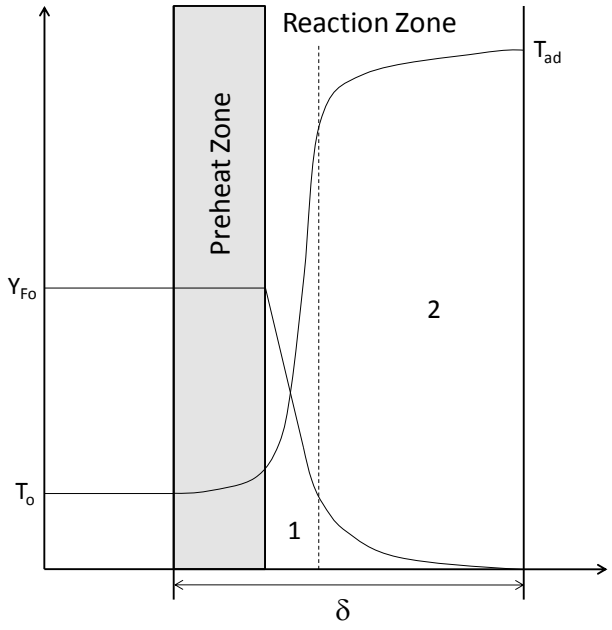

Figure 1 Temperature and fuel species profile across a flame.

In the preheat zone of a flame, the temperature of the reactants is increased by heat flux from the reaction zone. The preheat zone does not have much heat release as the majority of the reactions occur in the reaction zone that follows. The reaction zone can be divided into two distinct sections. The first section of the reaction zone, denoted by 1 in Figure 1, is a thin region of fast chemistry. This section is dominated by bimolecular reactions where the fuel molecules are quickly broken down, and many intermediate species are formed. This thin zone with large gradients provides the driving forces causing the flame to be self-sustaining. The secondary reaction zone, illustrated by region 2 in Figure 1, is dominated by three-body radical recombination reactions, which are much slower (Turns, 2000). This zone is much thicker than the fast-chemistry section.

To understand how the thermodynamic properties change from the reactants to the products, a one-dimensional, steady, planar flame with the reference frame fixed to the flame can illustrate the effects, as shown in Figure 2.

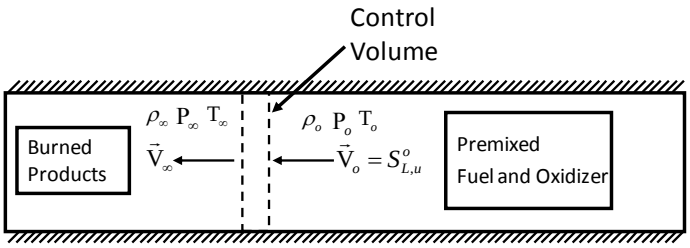

Figure 2 Control volume analysis for a steady, one-dimensional, planar flame.

The conditions before and after the flame are shown in Figure 2, with the unburned state shown to the right of the control volume and the burned state shown to the left of the control volume. The equations governing the propagation of a premixed laminar flame are mass conservation, species conservation, and energy conservation. Due to the fact that deflagrations are essentially constant pressure, the momentum equation does not govern them. The three governing equations that define the propagation of a premixed laminar flame are developed below and are based on three main assumptions (Turns, 2000):

- One-dimensional, steady flow.
- Kinetic and potential energies, viscous shear work, and thermal radiation are all neglected.
- Pressure is constant.

The conservation of mass equation reduces to Eq. (1) for one-dimensional, steady flow.

$$\frac{d\dot{m}''}{dx} = 0 \quad \rightarrow \quad \rho_o v_o = \rho_\infty v_\infty \tag{1}$$

In Eq. (1), $\dot{m}''$ is the mass flow rate, ρ_o is the unburned density, v_o is the unburned velocity, ρ_∞ is the burned density, and v_∞ is the burned velocity.

The conservation of species equation develops the change in species mass fraction, diffusion, and volumetric species production, shown in Eq. (2).

$$\dot{m}'' \frac{dY_i}{dx} + \frac{d}{dx}\left(\rho Y_i v_{i,diff}\right) = \dot{\omega}_i M_w \tag{2}$$

Here, $\dot{m}''$ is the mass burning rate per unit area, Y_i is the mass fraction of species *i*, ρ is the density of the mixture, $v_{i,diff}$ is the diffusion velocity of species *i*, $\dot{\omega}_i$ is the volumetric species production rate, and M_w is the molecular weight of the mixture.

The conservation of energy equation considers energy change due to chemical reactions, boundary conditions, and diffusion. The simplified equation for the assumptions listed is given by Eq. (3).

$$\dot{m}'' c_p \frac{dT}{dx} + \frac{d}{dx}\left(-k\frac{dT}{dx}\right) + \sum_{i=1}^{N} \rho\, Y_i v_{i,diff} c_{p,i} \frac{dT}{dx} = -\sum_{i=1}^{N} h_i \dot{\omega}_i M_w \tag{3}$$

In Eq. (3), c_p is the mixture specific heat, k is the thermal conductivity of the mixture, $c_{p,i}$ is the specific heat of the species *i*, and h_i is the enthalpy of species *i.* To solve these three equations and predict the laminar flame speed of a combustible mixture, numerical programs are typically used. In this study, the Premix module in Chemkin (CHEMKIN-PRO 15101, 2010) was used to solve the equations. In addition to the three governing conservation equations, there are several other relations and information that are needed including ideal gas equation of state, relations for diffusion velocities, temperature dependent

species properties, mixture property relations, chemical kinetic mechanism for $\dot{\omega}_i$'s, and boundary conditions.

CHAPTER III

HIGH-TEMPERATURE AND HIGH-PRESSURE FLAME SPEED FACILTY

3.1 Flame Speed Facility

The flame speed facility used in this study consists of two, constant-volume cylindrical vessels. The first vessel is made of aerospace-grade aluminum and has an internal diameter of 30.5 cm with optical access using two fused quartz windows about 20 cm in diameter. This vessel is the facility's original flame speed bomb where more details about the vessel can be found in de Vries et al. (2010) and Lowry et al. (2011). The other vessel used in this study is a newly developed stainless steel vessel capable of performing experiments at initial temperatures up to 600 K (620°F) and initial pressures up to 30 atm. The design and hardware details of the high-temperature and high-pressure vessel are discussed in more detail in the following sections.

The layout of the flame speed facility is shown in Figure 3. Each vessel has its own thermocouple to monitor the initial gas mixture temperature. Each gas mixture is made using the partial-pressure method via 0–1000 Torr and 0–500 psi (34 atm) pressure transducers. Two additional pressure transducers with the same pressure capability are located near the stainless steel vessel to accurately monitor gas pressures at elevated temperatures. The purity of each gas used in this study is shown in Table 1. Each gas component is filled and vented through a stainless steel manifold system, shown in Figure 4, which is controlled remotely by electro-pneumatic valves. For the experiments that required water as part of the premixed combustible mixture, distilled water was injected directly into the evacuated chamber volume as a liquid using a ground-glass syringe with a hypodermic needle and a septum mounted directly on the vessel. The water vaporized quickly and the pressure was allowed to stabilize within the heated vessel. Additionally, the gas mixture is ignited remotely from a separate control room. The ignition consists of an adjustable, constant-current power supply (GwInstek GPR-1810HD), a 10-μF capacitor, an automotive coil, and a solenoid switch. The spark is created across two sharpened electrodes that are 0.9-mm (0.035 in) diameter Alloy X rods and are set at a variable gap.

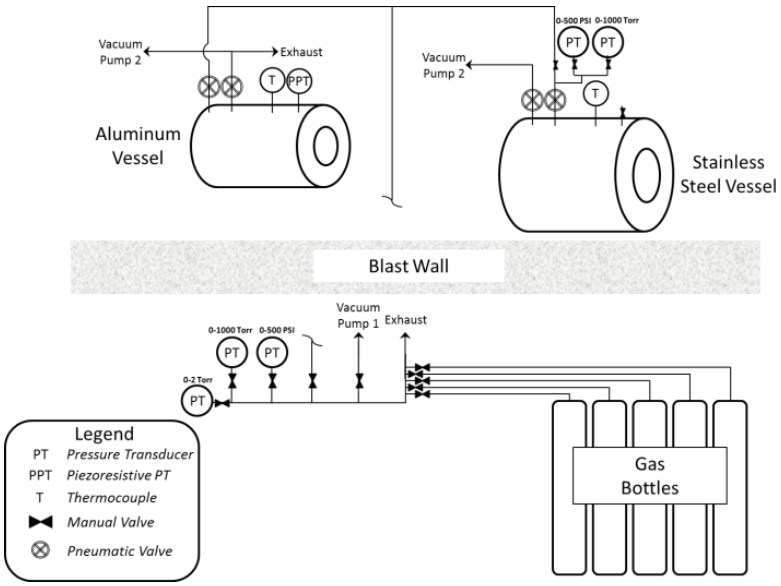

Figure 3 Layout of the flame speed facility at Texas A&M University.

Table 1 Gas purity summary

Gas	Grade	Purity
H_2	5.0	99.999%
CO	3.0	99.9%
O_2	UHP	99.999%
N_2	UHP	99.999%
He	UHP	99.999%

Figure 4 Mixing manifold for flame speed apparatus.

3.2 High-Temperature and High-Pressure Vessel Design

The design of a new high-temperature and high-pressure flame speed vessel required careful planning including the layout of the facility, the types of materials to be used, and the schematic drawings for custom machining. The setup and detailed description of several components for this facility are mimicked from the author's original, aluminum, cylindrical flame speed vessel facility and are further explained in Lowry et al. (2011). The flame speed facility has been upgraded to be able to perform experiments in both the original, aluminum flame speed vessel and the HTHP flame speed vessel, shown in Figure 5. A 1-ton crane had to be implemented due to the size and weight of the HTHP vessel. Therefore, the facility layout had to be re-designed to accommodate the new crane while still being able to perform experiments in both flame speed vessels and use its unique optical technique that requires a light source, two parabolic mirrors, and a high-speed camera, described in more detail in the Optical Technique section.

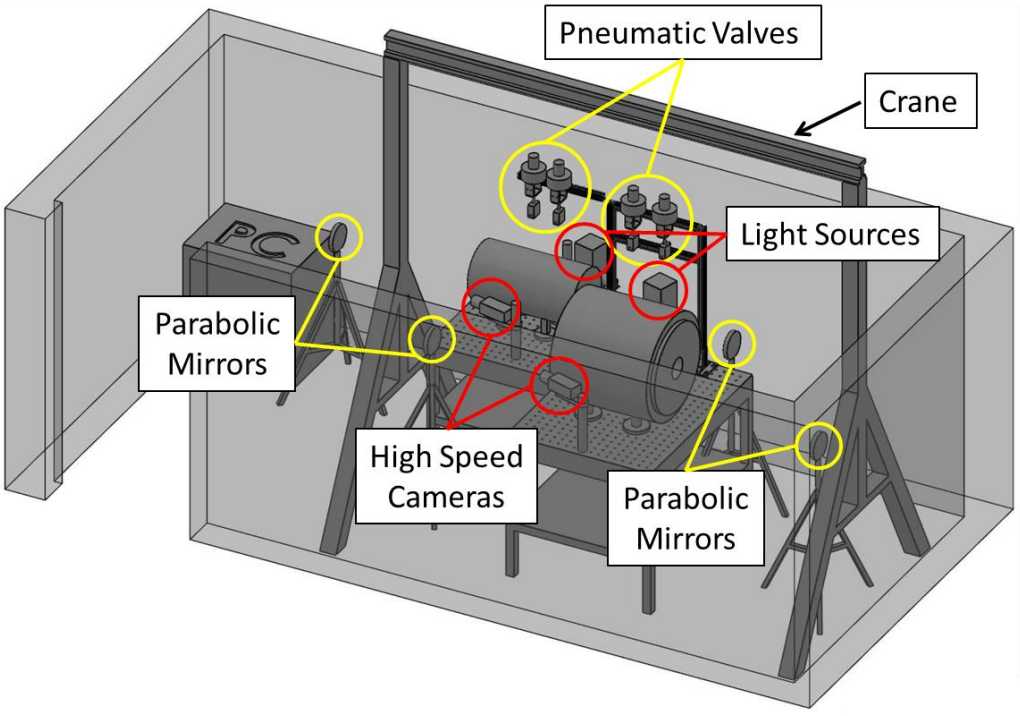

Figure 5 Schematic of flame speed facility configuration showing the new HTHP vessel (foreground) and the original flame speed vessel (background).

The cylindrical HTHP vessel was built according to the American Society of Mechanical Engineers (ASME) Boiler and Pressure Vessel Code (BPVC) sections II and VIII (American Society of Mechanical Engineers, 2000) and is made of 17-4PH, a high-strength and temperature-resistant stainless steel. It is comprised of the following main components: a thick-walled cylindrical body, two custom-designed flanges, two fused quartz windows, and two cylindrical lock plates. Figure 6 shows a 3-D model of the HTHP flame speed vessel general design while the detailed machine drawings are shown in the Appendix (Figure A 1-Figure A 4). The thick-walled cylindrical body has a 31.8-cm inner diameter with an 11.4-cm wall thickness. The two custom-designed flanges, each weighing nearly 181.4 kg (400 lb), contain a 12.7-cm diameter port for optical access and are diametrically sealed by Parker Parofluor ULTRA^{TM} O-rings. Each flange is fastened into the vessel by 12, ASTM A193 B7 bolts. The 20.3-cm diameter and 6.35-cm thick fused quartz windows sit within each flange and are each sealed by two Garlock Graphonic® gaskets. Each window is then clamped in place by a 30.5-cm outer diameter and 5.0-cm thick stainless steel lock plate.

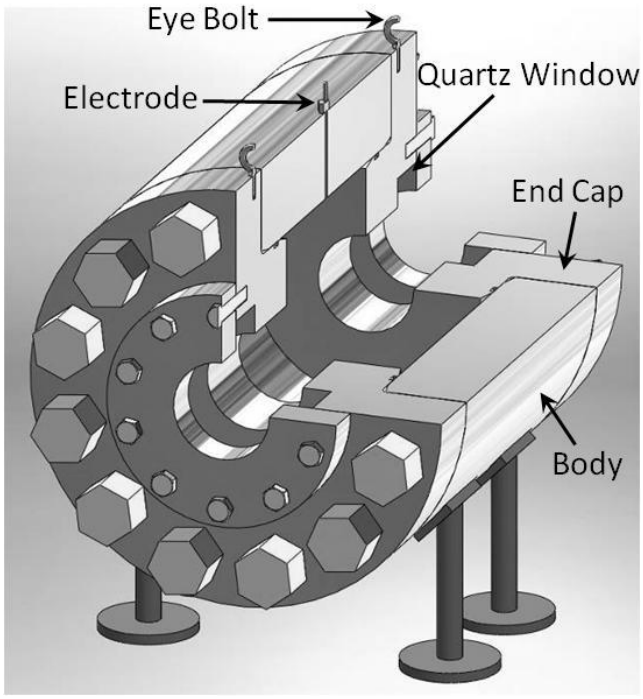

Figure 6 Cutaway representation of HTHP flame speed vessel.

3.3 High-Temperature and High-Pressure Vessel Hardware

The stainless steel chosen to develop the HTHP vessel, 17-4PH, was extensively researched to provide the greatest strength at the maximum operating temperature while remaining cost effective. The ultimate tensile strength of 17-4PH heat treated at the H1025 condition is about 1,070 MPa at room temperature, while the yield strength is about 1,000 MPa. This type of stainless steel maintains excellent strength properties with increased temperature. At 600 K (620°F), the maximum desired initial temperature, the strength properties of the stainless steel are expected to only lose about 20% of their tensile and yield strengths as shown in Figure 7 (U.S. Department of Transportation, 2003). These expected strength properties at 600 K (620°F) were used for stress and failure analysis calculations, shown in Figure 8 and Figure 9. Figure 8 shows the factor of safety plot for the end cap of the vessel with a minimum safety factor of 3.0, while Figure 9 shows the factor of safety plot for the body of the vessel with a minimum safety factor of 5.4. The minimum safety factor is indicated by red and the maximum safety factor is shown as blue.

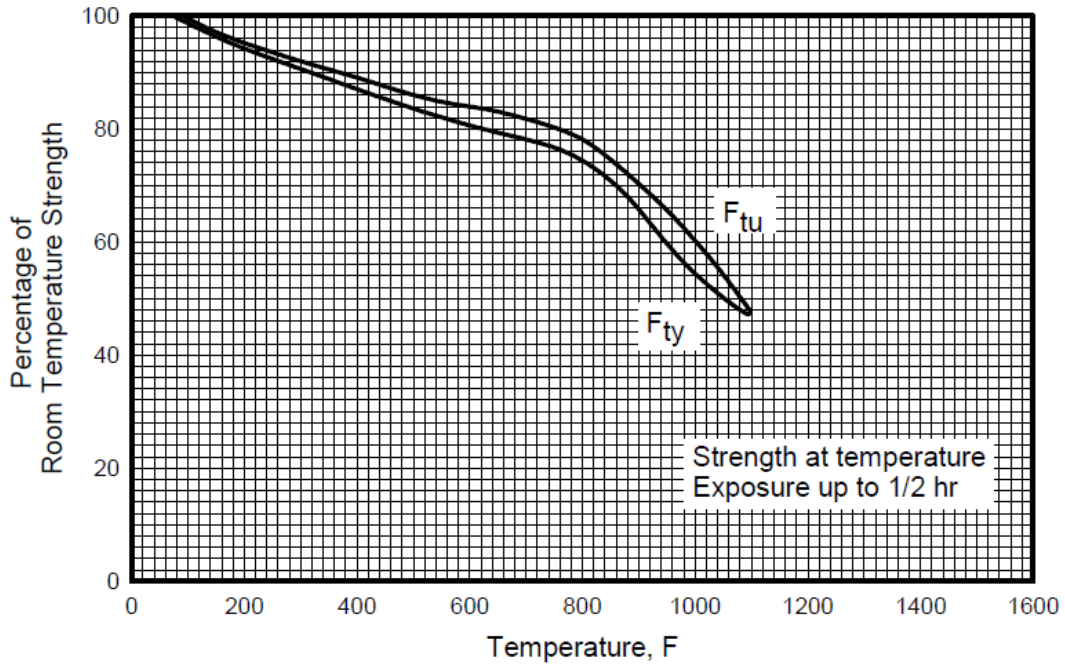

Figure 7 The strength relationship of 17-4PH stainless steel with temperature (U.S. Department of Transportation, 2003).

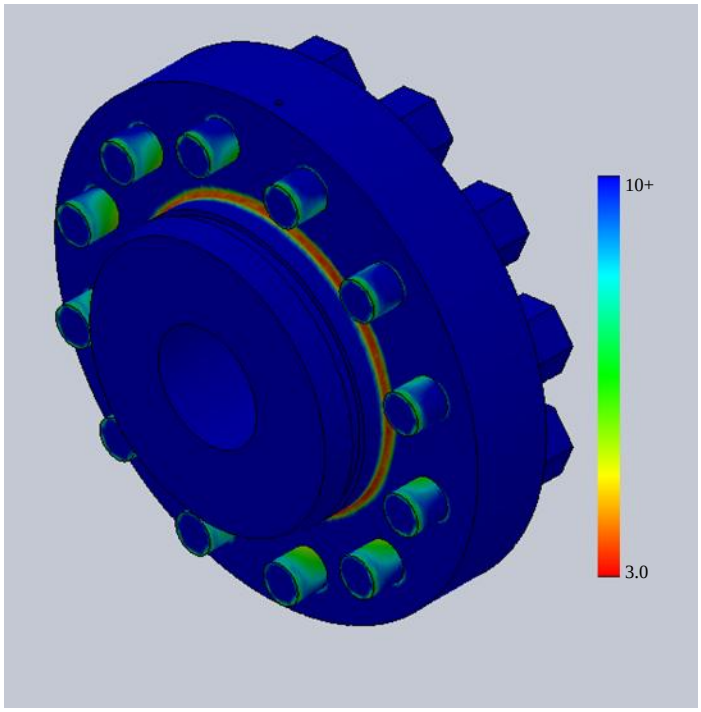

Figure 8 Factor of safety plot for the end cap with a minimum safety factor of 3.0.

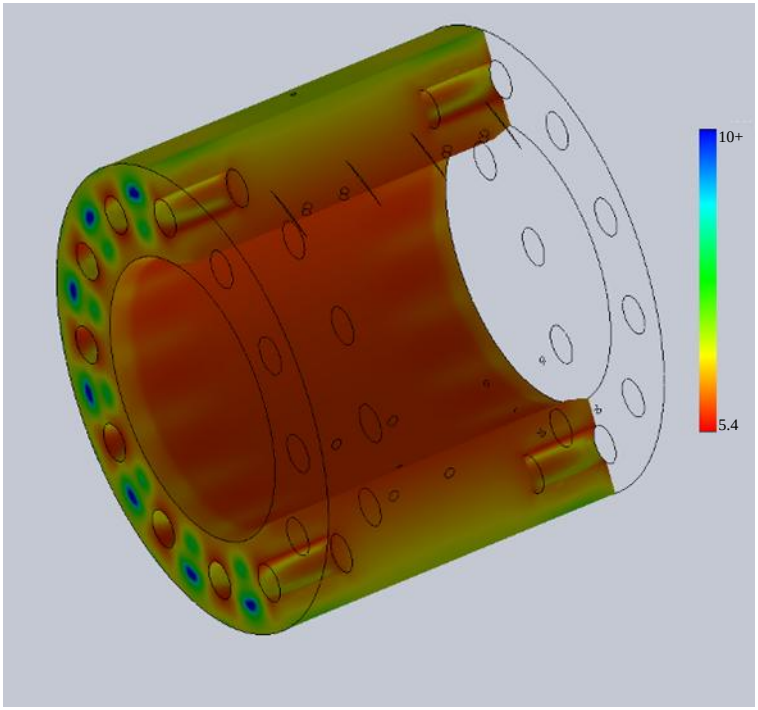

Figure 9 Factor of safety plot for the vessel body with a minimum safety factor of 5.4.

The pressure rating of the HTHP vessel was found using *Roark's Formulas for Stress and Strain* using the standards set by the ASME BPVC section II and VIII (Young and Budynas, 2002; American Society of Mechanical Engineers, 2000). According to these equations, the maximum stress expected with an internal pressure of 300 atm is 62.7 MPa in the circumferential direction. With a 20% decrease in yield strength of the material due to the initial temperature, this decreased yield strength would result in a factor of safety about 12 for the main body of the vessel. The end caps will be exposed to a maximum instantaneous force about 2,600 kN and are designed to minimize the amount of deflection to prevent bending on the window and to reduce the amount of stress in high-stress-concentration areas such as filleted corners. Additionally, this applied force provided enough information to design the type, quantity, and size of the bolts to safely enclose the vessel for experiments at a 30-atm initial pressure and a 600-K (620°F) initial temperature.

To have two flame speed vessels fully operational, additional equipment had to be added to the facility including pressure transducers, a vacuum pump, and a heating jacket. The two pressure transducers, 0-500 psi and 0-1000 Torr, reside between the high-pressure valve and a manual valve, as shown in Figure 3, to allow for low vapor pressure liquids to be accurately measured when injected into the vessel. These pressure transducers are designed to measure gases at high temperatures. Another addition to the gas manifold setup is a Leybold D16A vacuum pump, which is capable of achieving a vacuum as low as 0.1 mTorr. This pump is strictly used to vacuum the vessel once most of the combustion products have been exhausted by the other vacuum pump to continuously achieve a low vacuum pressure. Finally, the heating control system was designed to produce a high temperature of 350°C. The heating control system consists of a four-piece heating jacket, temperature controller, and a thermocouple which strictly monitors the temperature of the flame speed vessel's wall. The set point temperature on the controller can be adjusted from 25°C to 350°C by one-degree increments. This heating system allows for experiments to be performed over a wide range of initial gas temperatures.

3.4 Optical Technique

The experiment is visualized using a Z-type schlieren system as described by Settles (2006). Figure 10 shows a schematic of the optical setup. The source of light is generated by a mercury arc lamp that is passed through a condenser lens before reflecting off the first 15.2-cm, f/8 parabolic mirror. The reflected light is passed through the vessel where it is reflected off a second 15.2-cm, f/8 parabolic mirror towards a high-speed camera. A circular pinhole aperture, adjustable from 1 to 11 mm diameter, is used to cut off the light before entering the camera to intensify the density gradients as the flame spherically grows outwardly. The two high-speed cameras used in this study to capture the event were a Photron FastCam SA 1.1 and a Cooke Corporation PCO 1200-hs. Example images from this study are shown in Figure 11 to demonstrate the high-quality picture and the increase of flame instability with increasing pressure.

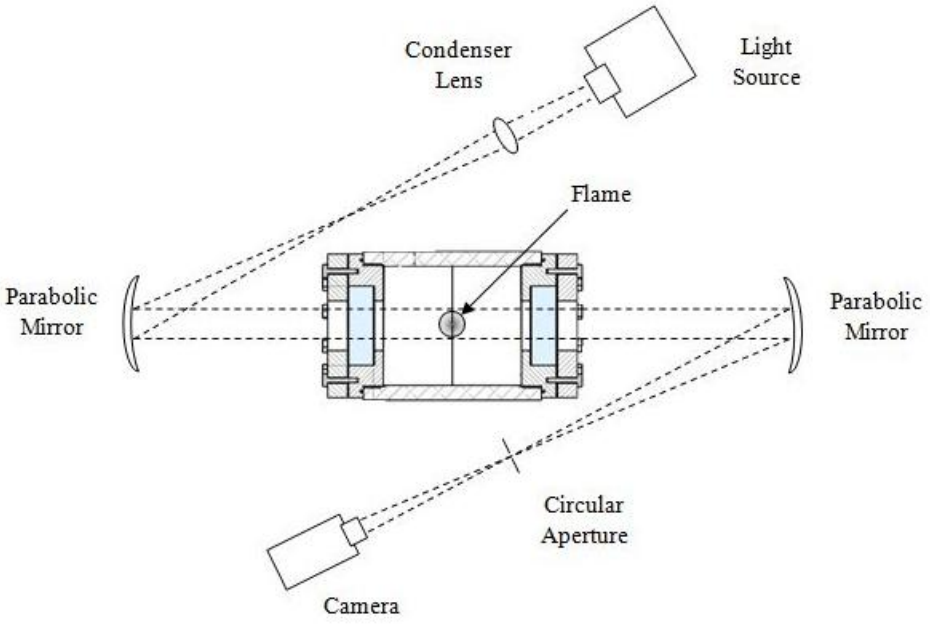

Figure 10 Optical setup for high-speed schlieren system.

.

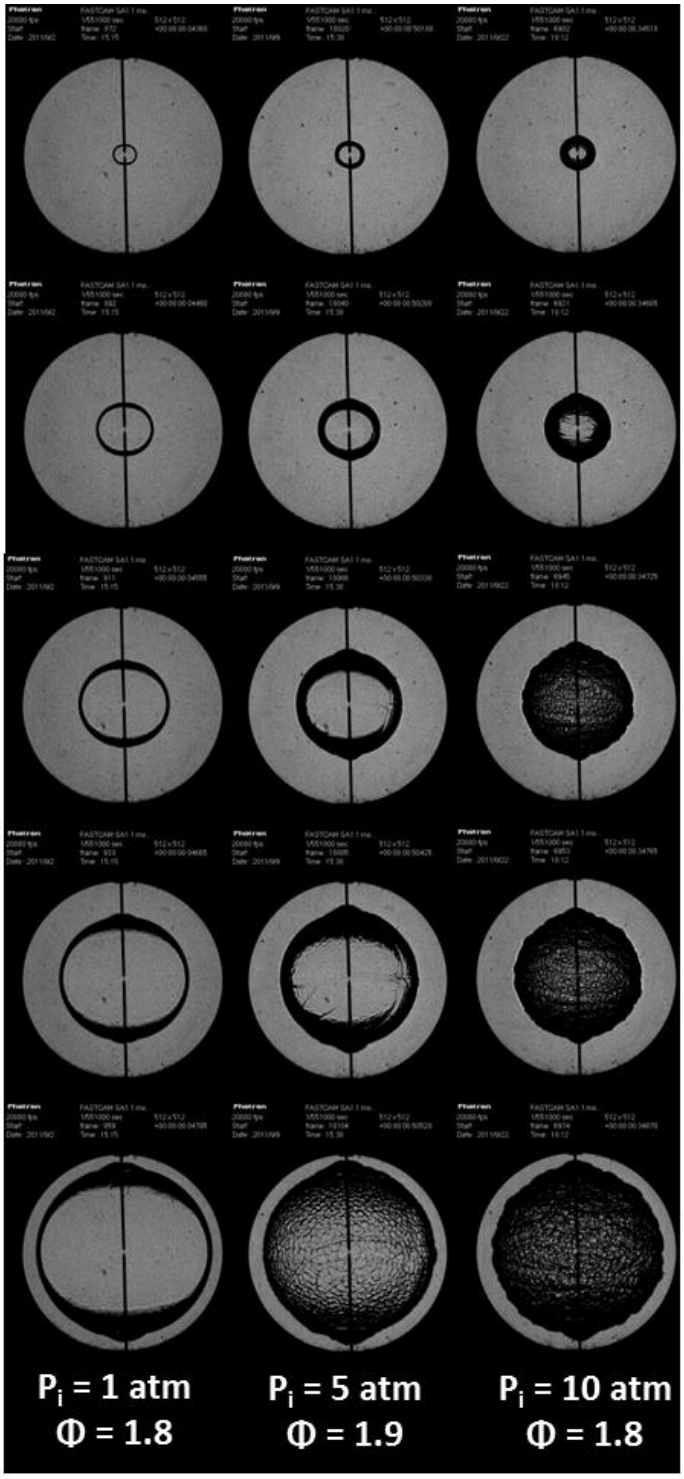

Figure 11 Flame images for 1-atm (left), 5-atm (middle), and 10-atm (right) 50:50 H_2:CO at 298 K. The oxidizer for the atmospheric experiment is air, while the oxidizer for the 5- and 10-atm experiments is 1:7 O_2:He.

3.5 Validation

To validate the operational capability of the high-temperature and high-pressure (HTHP) vessel several experimental studies where performed including temperature uniformity, hydrogen mixture experiments at elevated pressure and temperature, syngas mixture experiments at elevated pressures, and syngas diluted with water.

3.5.1 Temperature

Achieving and maintaining a uniform temperature within the vessel is extremely important for conducting experiments using an outwardly propagating flame. For example, regions of higher or lower temperature could cause the flame to speed up or slow down in an undesirable manner, potentially impacting the inferred laminar flame speed. Figure 12 shows the layout of the thermocouples in the vessel and presents a sample of the thermocouple readings at a set point of 100°C. The heating jacket was set at determined temperatures to study the differences between the set point temperature, vessel thermocouple reading, and the actual gas temperature. Several individual thermocouples were strategically placed inside the flame speed vessel to measure the radial change in temperature. Since all of the thermocouples measuring the actual gas temperature were within 1.0°C, those temperatures were averaged and compared to the vessel thermocouple reading as shown in Figure 13. A linear regression line is shown to demonstrate that an accurate initial gas temperature can be determined from the vessel thermocouple.

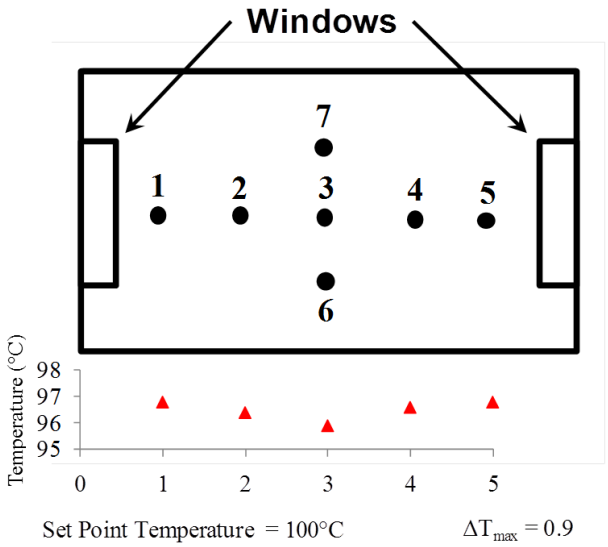

Figure 12 Thermocouple setup in the vessel and a sample of temperature readings from a set point of 100°C.

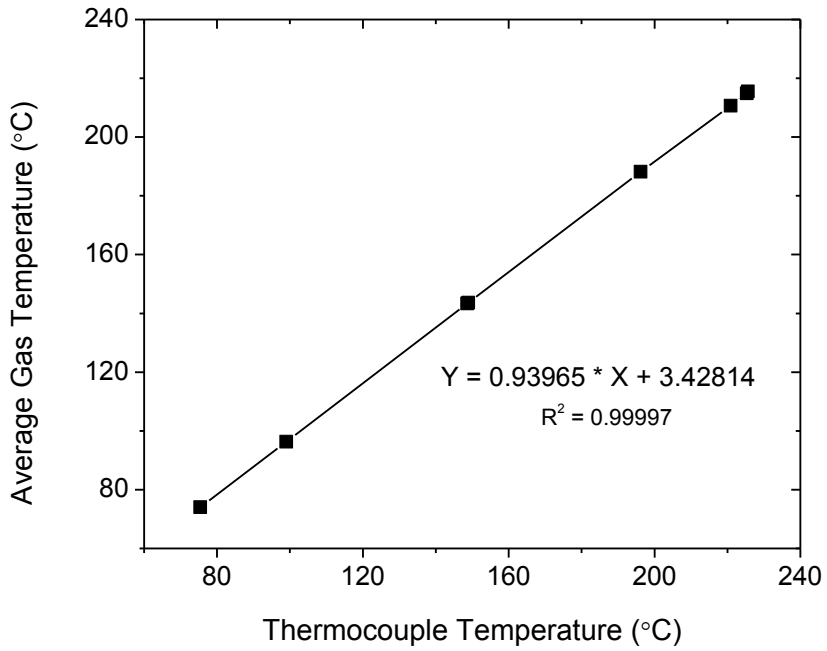

Figure 13 A linear correlation was developed by comparing the average gas temperature inside the flame speed vessel and the vessel thermocouple reading to provide an accurate method to set the initial temperature. The average gas temperature comes from seven different thermocouples placed at different radial positions within the vessel.

3.5.2 Hydrogen

The mixture compositions performed in the cylindrical bomb include hydrogen diluted with air at atmosphere pressure and three initial temperatures, and hydrogen diluted with helium at two elevated pressures and three temperatures, as shown in Table 2. For all elevated-pressure experiments, the oxidizer ratio was adjusted to a 7:1 He:O_2 ratio to increase the Lewis number of the mixtures and minimize thermal-diffusive instabilities. This ratio was chosen because it produces an adiabatic flame temperature comparable to that of air for a given fuel. This effect is illustrated in Figure 14 with the adiabatic flame temperature of hydrogen reacting with several oxidizer compositions over a range of equivalence ratios. Experiments with initial pressures of 1 atm were performed with standard air. Additionally, all initial temperatures have an uncertainty of ±3 K. Table A 1 and Table A 2 in the appendix provide the raw experimental data for the hydrogen conditions studied.

Table 2 Hydrogen experimental conditions for measuring laminar flame speed.

H_2:CO	Temperature (K)	Pressure (atm)
100:0	298	1
		5
		10
	373	1
		5
	443	1
		5

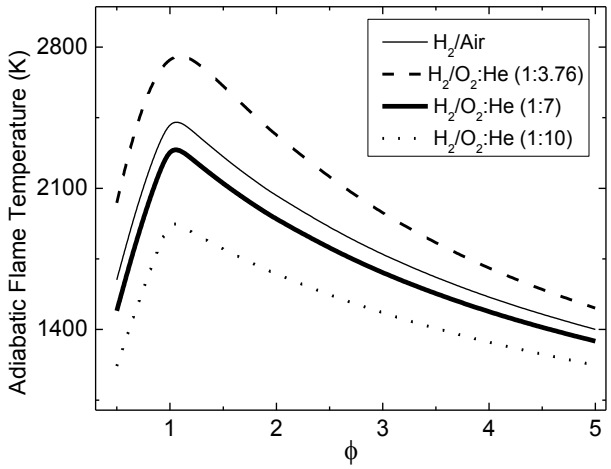

Figure 14 Adiabatic flame temperature comparison between standard air and various O_2:He ratios reacting with pure H_2. The 1:7 ratio produces adiabatic flame temperatures close to an air mixture.

Figure 15 demonstrates an extensive literature comparison for atmospheric hydrogen-air at room temperature between the data herein and the experimental work done by Egolfopoulos and Law (1990); Vagelopoulos et al. (1994); Aung et al. (1997); Tse et al. (2000); Kwon et al. (2001); Lamoureux et al. (2003); Dahoe (2005); Verhelst et al. (2005); Burke et al. (2009); and Pareja et al. (2010). Since the H_2-O_2 chemical kinetic system has been well studied for the past few decades, it is expected that the agreement would be quite well between the data herein and previously published data, as shown in Figure 15. However, unified agreement begins to dissipate at an equivalence ratio of about 1.0 and above. Additionally, when Figure 15 is magnified to equivalence ratios below 1.0, as shown in Figure 16, a potentially large variance exists amongst published flame speed data in a regime that typically has a distribution of about ± 2 cm/s, such as the flame speed of methane-air (Lowry et al., 2011). The model exhibits excellent agreement with the new data of this study, reproducing it across the complete range of equivalence ratios.

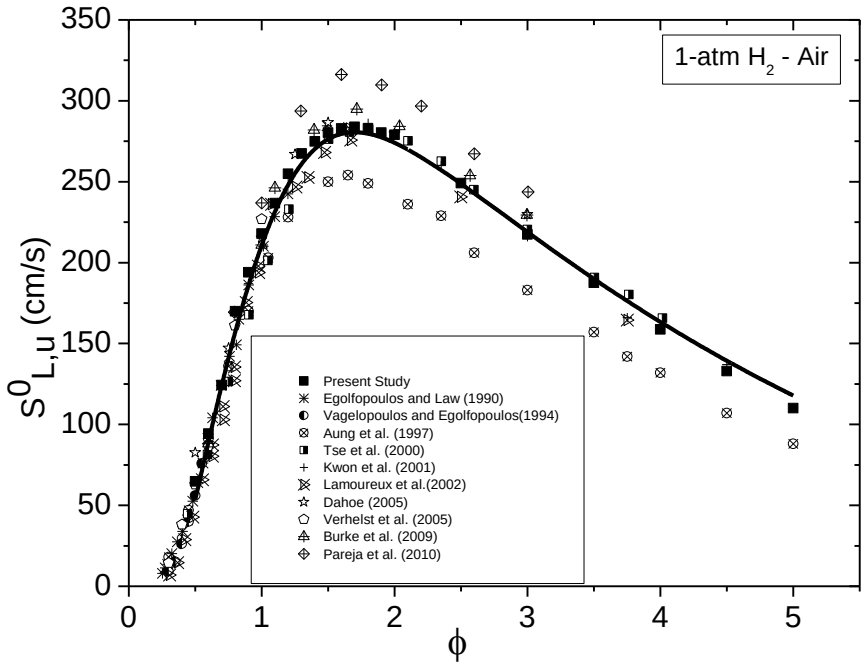

Figure 15 Atmospheric hydrogen-air literature comparison to the data herein and the chemical kinetics model at standard temperature.

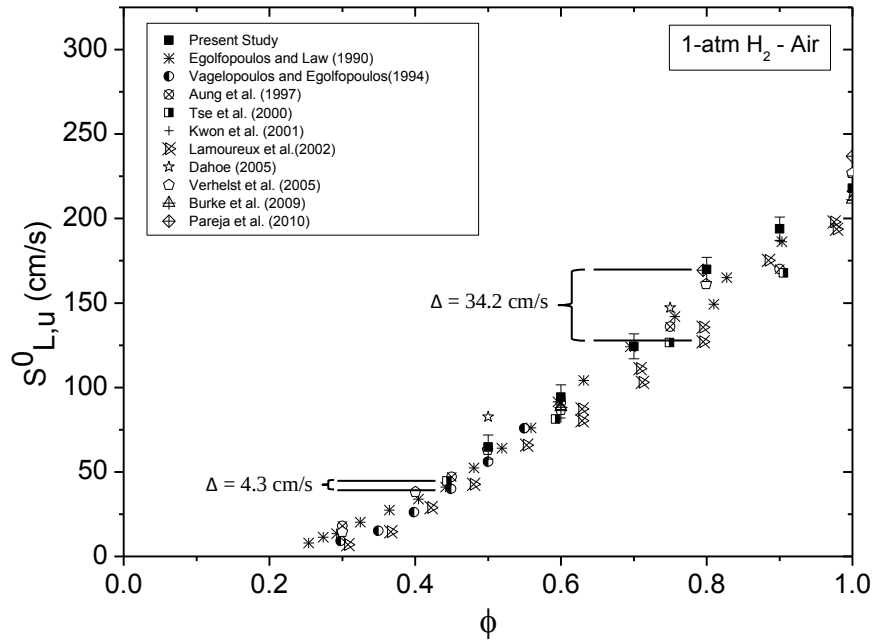

Figure 16 Atmospheric hydrogen-air at equivalence ratios less than 1.0 demonstrating the increased distribution of laminar flame speed data.

Figure 17 explores the effects of pressure on hydrogen diluted with 7:1 He:O_2. With limited literature available at these pressures, this plot shows good agreement between the experimental data herein and data from Tse et al. (2000) at 5 atm. The model agrees quite well with the 5-atm data obtained in this study, particularly under lean conditions and richer conditions ($\phi \geq 2$). However, the peak flame speed is underpredicted, with the model reproducing the existing data more accurately. The agreement deteriorates slightly with increasing pressure, with the model predicting a larger inhibiting effect of pressure than experimentally measured at an equivalence ratio around 1.5. Once again, the agreement at richer conditions is excellent.

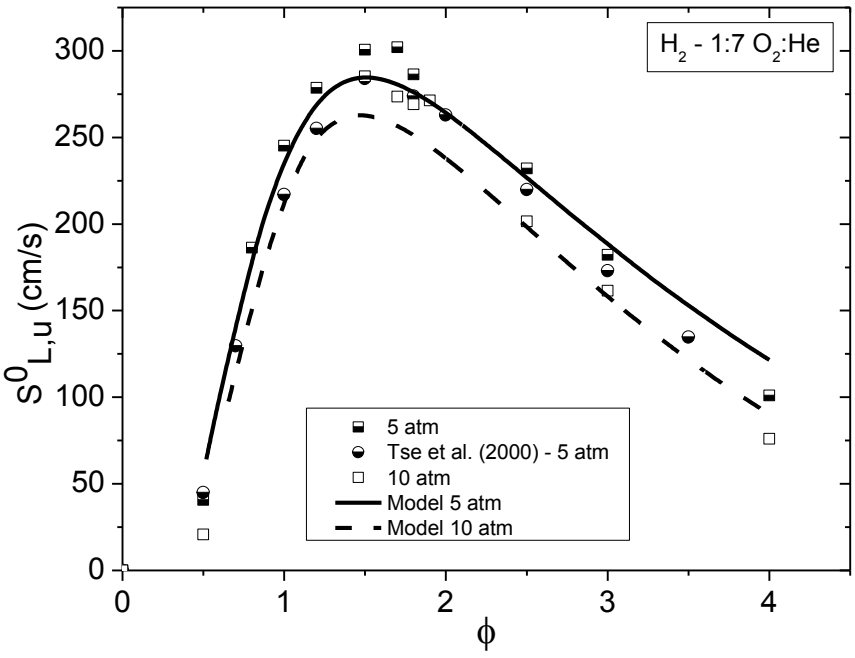

Figure 17 Hydrogen diluted with 7He:O_2 at 5 and 10 atm compared with the chemical kinetics model and data from Tse et al. (2000).

Figure 18 and Figure 19 show the influence of initial pressures at elevated temperatures on the laminar flame speed. Hu et al. (2009) demonstrate excellent agreement for atmospheric hydrogen at elevated temperatures up to 443 K. As temperature increases for both initial pressure conditions, the laminar flame

speed increases substantially. Model agreement at 1 and 5 atm and elevated temperatures is excellent across the complete range of equivalence ratios.

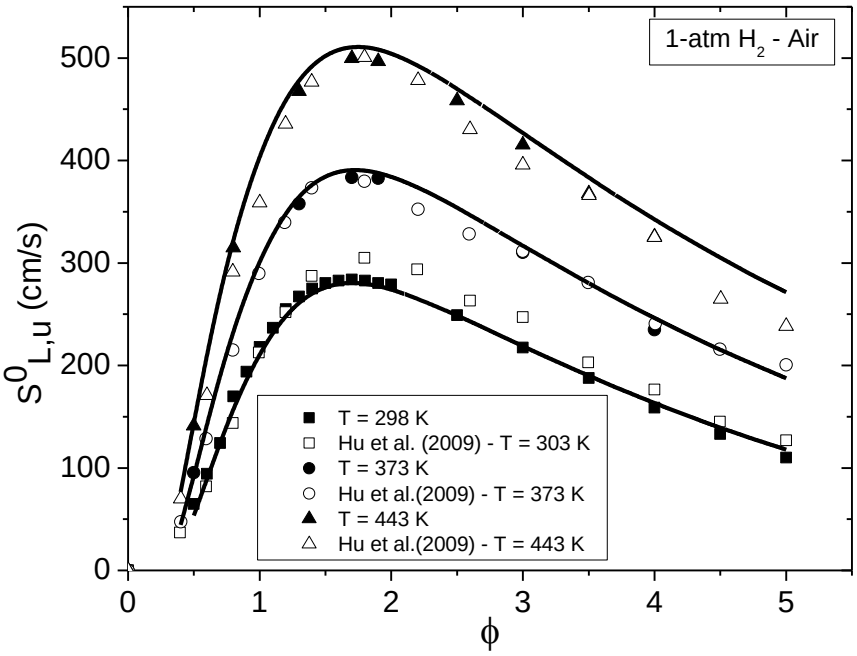

Figure 18 Comparison of atmospheric hydrogen-air data herein (solid symbols), data from Hu et al. (2009), and the chemical kinetics model at elevated temperatures.

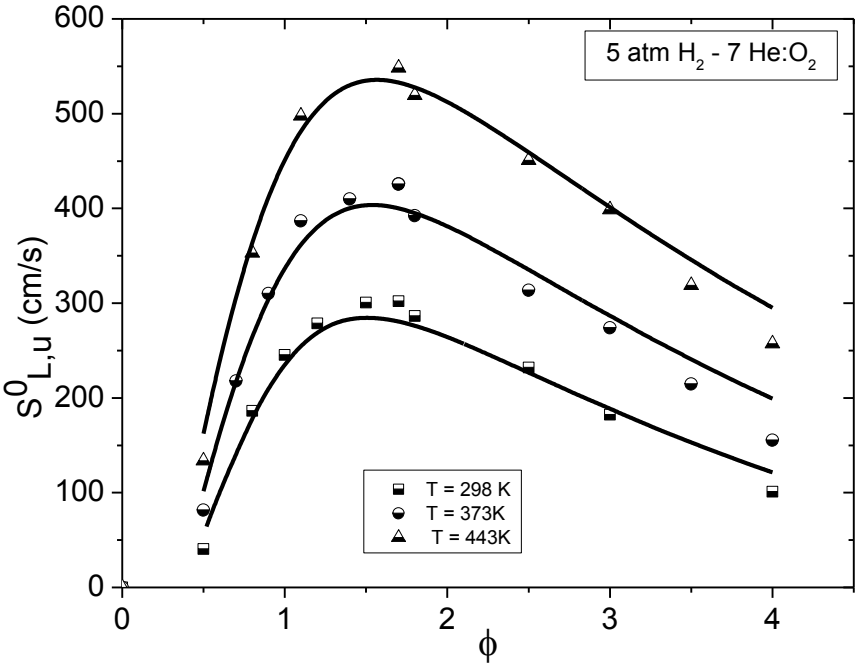

Figure 19 Laminar flame speed of hydrogen diluted with 7He:O_2 at 5 atm and elevated temperatures compared to the chemical kinetics model.

3.5.3 Syngas

Figure 20 and Figure 21 provide a baseline set of data for a common syngas (model) mixture with a 50:50 H_2/CO composition at 1 atm and elevated pressures, respectively. The atmospheric syngas data herein, shown in Figure 20, is compared with previously published data from McLean et al. (1994); Hassan et al. (1997); Sun et al. (2007); Natarajan et al. (2005); Burke et al. (2007); Prathap et al. (2008); Dong et al. (2009); and Bouvet et al. (2011). These data show a similar trend in agreement as seen with atmospheric hydrogen, where good agreement exists on the fuel-lean side, and discrepancies increase as the mixture becomes fuel rich. Once again, the model agreement with the data obtained in this study is excellent, with only minor disparities arising at high equivalence ratios. At elevated pressures, the 50:50 H_2:CO data herein are compared with Sun et al. (2007) and Natarajan et al. (2009) in Figure 21. Overall agreement at both pressures is quite good. There are some discrepancies around the peak flame speed at 10 atm which is

under further investigation. This disagreement is also highlighted by the model, which predicts considerably lower reactivity at the elevated pressures, while reproducing the 5-atm data quite well.

Iron pentacarbonyl, $Fe(CO)_5$, impurities have been reported to have a potential influence on the flame speed of syngas mixtures (Bouvet et al., 2011; Chaos and Dryer, 2008). Rumminger et al. (2000) studied how iron pentacarbonyl changes the chemical kinetic reaction pathways and rates for H_2/CO/air flames and demonstrated that it can lead to a decrease in flame propagation. Chaos and Dryer (2008) and Bouvet et al. (2011) show that the laminar flame speed of syngas mixtures has the largest potential to be affected in the fuel-rich regime, but conclude that the large discrepancies between other published syngas flame speed values cannot be fully explained by iron pentacarbonyl. Based on the suggestions in Bouvet et al. (2011) and Williams and Shaddix (2007), the ultra-high purity carbon monoxide was stored in an aluminum bottle, and Teflon tubing was used for transportation to minimize any effect by iron pentacarbonyl.

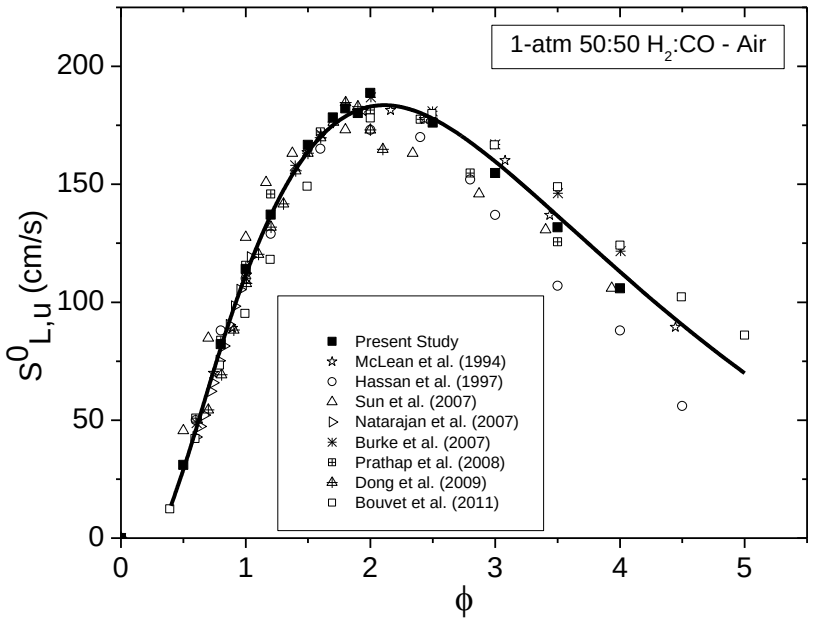

Figure 20 Literature comparison of atmospheric 50:50 H_2:CO-Air with the data herein and the chemical kinetics model.

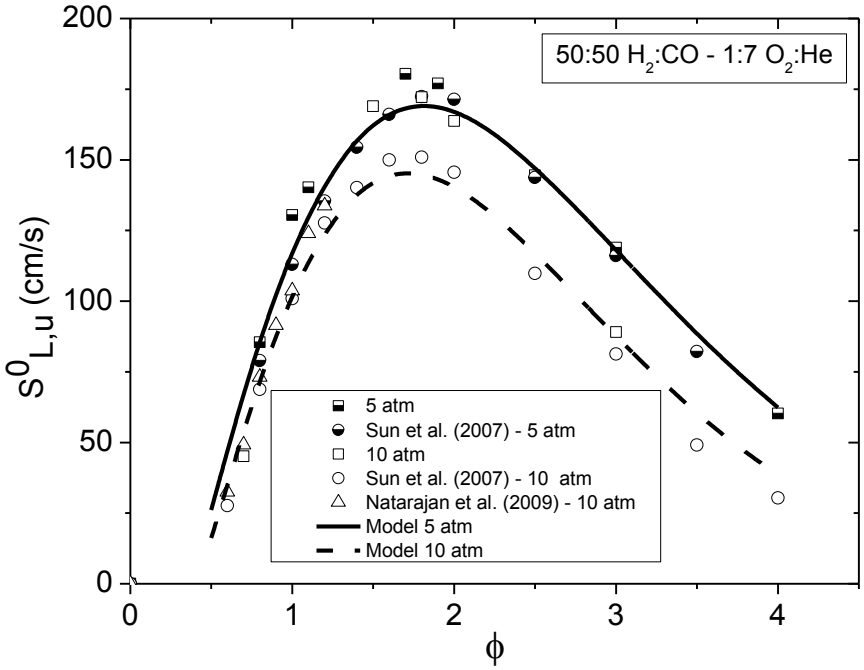

Figure 21 Comparison of 5- and 10-atm 50:50 H_2:CO diluted with 1:7 He:O_2 with literature data and the chemical kinetics model.

3.5.4 Syngas with Water Dilution

It is important to validate moist mixtures to demonstrate the accuracy of the chosen method of introducing steam into each mixture. Therefore, an experimental series was chosen based on previously published data from Das et al. (2011). Figure 22 compares atmospheric 5:95 H_2:CO diluted with 7.5% steam at 323 K data to the data of Das et al. (2011) and to the chemical kinetics model. The data in this figure are shown with experimental error bars demonstrating the relative uncertainty of the laminar flame speed measurements. The relative uncertainty is similar for the other figures presented below but are not shown to better display the data trends. The experimental data set shows good agreement, within 2 cm/s, while the model also exhibits excellent predictive behavior at these fuel-lean conditions.

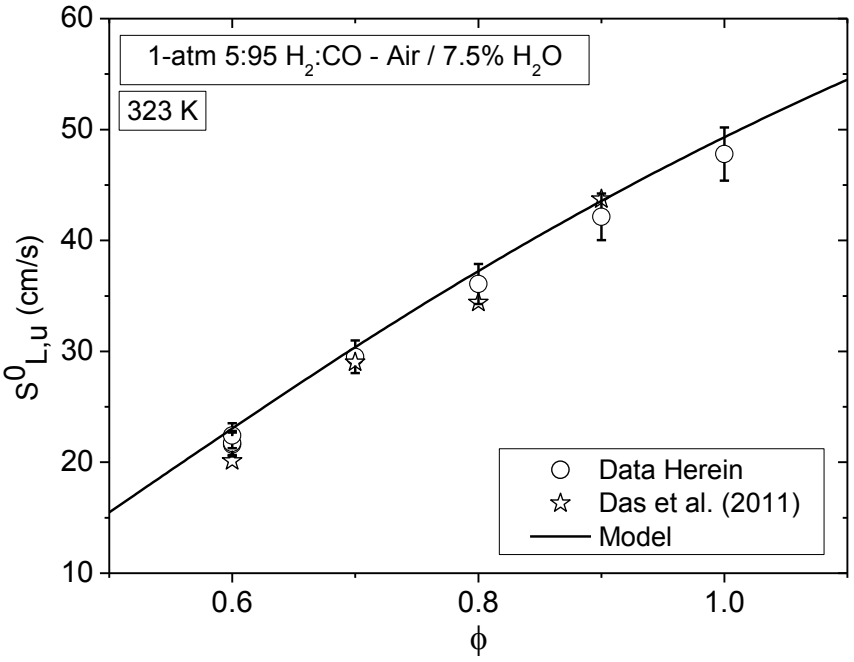

Figure 22 Laminar flame speed for atmospheric 5:95 H_2:CO diluted with 7.5% H_2O at 323 K for the data herein, the data of Das et al. (2011), and the chemical kinetics model.

CHAPTER IV

ANALYSIS AND UNCERTAINTY

4.1 Data Interpretation

When measuring the laminar flame speed of a fuel-oxidizer mixture using a constant-volume vessel, it is important to ensure that the pressure remains constant for the duration of the measurement to avoid non-ideal pressure effects. The pressure remained constant during the measurement of the flame propagation because the vessel has a large internal diameter. A normalized pressure trace as a function of time is shown in Figure 23. A sample of flame images are also shown with the trace marking their relative times that the flame measurements were taken.

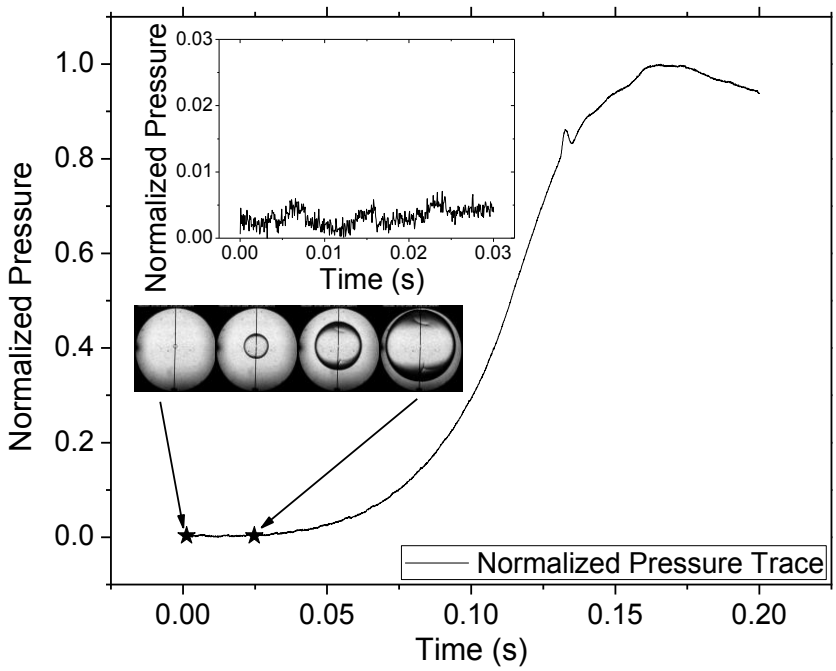

Figure 23 Experimental pressure trace showing time period of measurement. The inset figure shows a closer view of the constant-pressure measurement time period.

After each experiment, the high-speed images are post processed using Matlab. A code has been developed and implemented by a fellow colleague, Travis Sikes, to track the growth of the spherical flame

in a similar manner as described by Lowry et al. (2011). Figure 24a shows a sample image of how the contrast of the image is changed so as to locate the outside edge of the flame, and Figure 24b displays the original flame image with the flame edge detection and the six radial track points used to fit in a Euclidean circle algorithm.

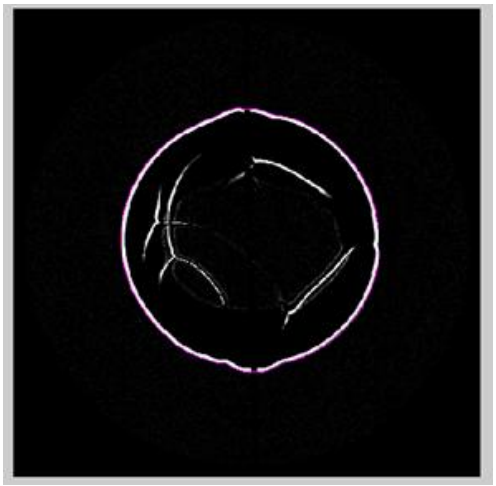

(a)

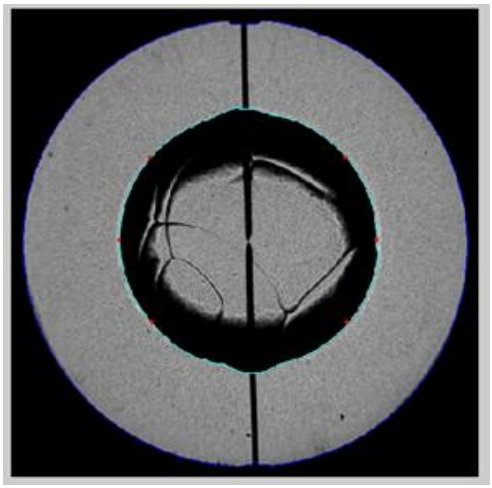

(b)

Figure 24 Images from the flame detection program. (a) The contrast of the image is changed to locate the edge of the flame (b) The original image is shown with the edge detection.

In this study, radii chosen for analysis are carefully determined to reduce any effects caused by the spark or by confinement. The typical radii used in the analysis correspond to less than 30% of the inner radius of the vessel. Therefore, the effect of confinement can be neglected for flame radii used in this study with less than 3% error (Burke et al., 2009). Flame images were converted into flame radii by using the methodology outlined in Figure 25. More detailed information on this technique is available in de Vries (2009).

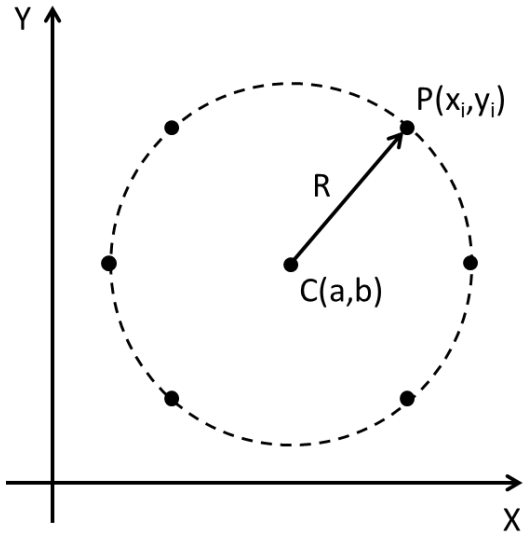

Figure 25 Graphical display of the six radial track points to demonstrate how the algorithm functions.

A best-fit algorithm using a least-squares estimator based on the Euclidean distance between the point and the circle, given by Eq. (4), was used.

$$J = \sum_{i=1}^{n} (d_i - R)^2 \quad \textbf{(4)}$$

Here, $d_i = \sqrt{(x_i - a)^2 + (y_i - b)^2}$, the Euclidean distance between the point P(x_i, y_i) and the center of the circle C(a,b) with a radius, *R*. This geometric definition of a circle can also be expressed as an algebraic equation, Eq. (5), which will allow for a much quicker and stable numerical estimation (Chernov, 2010).

$$A(x^2 + y^2) + Bx + Cy + D = 0 \quad \textbf{(5)}$$

Where A $\neq$ 0 and $B^2 + C^2 - 4AD > 0$. The algorithm used in this study uses the Taubin algorithm to minimize *J* by using the following numerical estimation with *n* data points (Chernov, 2010).

$$F(a,b,R) = \frac{n\sum_{i=1}^{n}\left[(x_i-a)^2+(y_i-b)^2-R^2\right]^2}{4\sum_{i=1}^{n}[(x_i-a)^2+(y_i-b)^2]} \quad \textbf{(6)}$$

This geometric definition can be converted to an algebraic equation using Eqs. (7-9) (Chernov, 2010).

$$a = \frac{-B}{2A} \quad \textbf{(7)}$$

$$b = \frac{-C}{2A} \quad \textbf{(8)}$$

$$R = \frac{B^2+C^2-4AD}{4A^2} \quad \textbf{(9)}$$

This fitting methodology allows for the center of the circle to be tracked and, therefore, can accommodate translations and rotations. Additionally, the Taubin algorithm is highly stable and is five to ten times faster than a typical geometric algorithm.

The instantaneous flame radius given by the image post-processing is analyzed using the linear relationship given by Eqs. (10-13) (Markstein, 1964; Dowdy et al., 1990; Brown et al., 1996).

$$S_b = S_b^o - L_{m,b}\alpha \quad \textbf{(10)}$$

Where S_b is the burned, stretched flame speed, S_b^o is the burned, un-stretched flame speed, $L_{m,b}$ is the burned Markstein Length, and α is the flame stretch defined by

$$\alpha = \frac{1}{A}\frac{dA}{dt} = \frac{1}{4\pi R^2}\frac{d\left(4\pi R^2\right)}{dt} = \frac{2}{R}\frac{dR}{dt} \quad \textbf{(11)}$$

After substituting Eq. (11) into (10), the result can be integrated to give Eq. (12), where R_f is the instantaneous flame radius and *t* is the corresponding time.

$$R_f = S_b^o t - 2L_{m,b}\ln\left(R_f\right) + const \quad \textbf{(12)}$$

The un-stretched flame speed S_b^o and Markstein length $L_{m,b}$ are then obtained by using linear regression. The un-burned, un-stretched flame speed $S_{L,u}^o$ and Markstein length $L_{m,u}$ are found by dividing the burned values, S_b^o and $L_{m,b}$ extracted from Eq. (12), by the density ratio across the flame given by Eq. (13).

$$\sigma = \frac{\rho_u}{\rho_b} \tag{13}$$

The density ratio was calculated using the Equilibrium module in Chemkin (CHEMKIN-PRO 15101) with the authors' chemical kinetics model as the input.

4.2 Uncertainty Analysis

The uncertainty analysis performed in this study takes into account both systematic and random uncertainties using the methods outlined by Moffat (1988). The total experimental uncertainty is given by Eq. (14), where B_{SL} is the systematic uncertainty and P_{SL} is the random uncertainty at a 95% confidence interval.

$$U_{S_L} = \sqrt{B_{S_L}^2 + P_{S_L}^2} \tag{14}$$

The systematic uncertainty includes u_i, the fixed error for each variable x_i, and S_L the relationship between the flame speed and each variable x_i is shown below.

$$B_{S_L} = \sqrt{\sum_{i=1}^{n}\left(\frac{\partial S_L(x_i)}{\partial x_i}u_i\right)^2} \tag{15}$$

A relationship between each independent variable and the flame speed had to be known to use this definition of the systematic uncertainty. Using the experimental and computational results of this study, a relationship of the following form is proposed, where T is the initial temperature in kelvin, and ϕ is the equivalence ratio. Table 3 and Table 4 provide the correlation constants (a, b, c, d, e, p, r, s) for the test conditions performed in the Design of Experiments methodology for ϕ less than 2.0 and ϕ greater than 2, respectively (further details on these experiments are presented later in this thesis).

$$S_{L,u} = (a + b\varphi + c\varphi^2 + d\varphi^3 + e\varphi^4)\left(\frac{T}{298}\right)^{(p+q\varphi+r\varphi^2+s\varphi^3)} \tag{16}$$

Table 3 Correlation constants for ϕ less than 2.0.

0.5<ϕ<2.0	a	b	c	d	e	p	q	r	s
Experiment 1	-27.668	91.437	-9.096	-10.229	2.589	2.457	-1.858	1.121	-0.226
Experiment 2	-109.573	302.483	-25.787	-45.287	10.262	3.389	-3.553	2.178	-0.426
Experiment 3	-123.59	271.10	283.85	-286.39	62.48	3.96	-4.34	2.55	-0.48
Experiment 4	-195.828	577.567	87.573	-221.425	53.430	4.088	-4.540	2.665	-0.510
Experiment 5	-63.139	213.421	-98.932	16.767	-0.767	3.670	-4.134	2.620	-0.524
Experiment 6	-94.233	199.319	156.111	-159.800	33.154	4.613	-5.705	3.622	-0.720
Experiment 7	-74.152	213.208	142.471	-138.823	28.135	3.505	-3.101	1.763	-0.330
Experiment 8	-393.614	1343.740	-624.907	52.722	13.518	4.699	-6.198	4.033	-0.839
Experiment 9	-64.566	215.758	-114.690	30.213	-3.611	3.860	-4.760	3.139	-0.668

Table 4 Correlation constants for ϕ greater than 2.0.

2.0≤ϕ<5.0	a	b	c	d	p	q	r
Experiment 1	-14.675	92.282	-26.341	1.975	1.699	-0.393	0.114
Experiment 2	160.686	94.907	-48.712	4.940	1.823	-0.397	0.145
Experiment 3	380.23	-44.13	-10.92	1.55	1.88	-0.21	0.07
Experiment 4	443.262	17.142	-27.850	2.855	1.619	-0.032	0.030
Experiment 5	45.102	71.546	-30.733	3.028	2.437	-0.649	0.192
Experiment 6	286.381	-23.362	-20.902	2.947	2.727	-0.813	0.251
Experiment 7	163.123	149.323	-59.241	5.299	1.658	-0.200	0.104
Experiment 8	638.663	-82.552	-15.741	2.399	1.742	-0.200	0.096
Experiment 9	-20.446	120.047	-39.164	3.389	2.736	-1.106	0.267

The uncertainty of each variable in the flame speed correlation was performed by assuming the worst case of error for the pressure. Since the mixtures were made using a partial pressure method, the error in pressure has a direct influence on the flame speed and an indirect influence through the equivalence ratio. The uncertainty of each transducer used is 0.25% of the reading for the MKS 0-1,000 Torr transducer and 0.15% of the reading for the 0-500 psi Setra transducer. This makes the MKS transducer more accurate and, therefore, it was used when the component pressure was less than 1,000 Torr.

The random uncertainties in this study are described by Eq. (17). Here $t_{M-1,95\%}$ is the student t-value at 95% confidence interval with (*M-1)* repeated experiments and S_{SL} is the standard deviation of the *M* repeated experiments.

$$P_{S_L} = \left(\frac{t_{M-1,95\%}\, S_{SL}}{\sqrt{M}}\right) \quad \textbf{(17)}$$

The precision uncertainty was measured for three different experimental mixtures that were repeated five times. The average of the three precision uncertainties was used as the precision uncertainty for all of the experiments performed within this study. The total absolute uncertainty in this study covered a large range, from as little as 4.0 cm/s to 16.7 cm/s considering all of the cases investigated. Uncertainty bars are left off of the plots to allow for clear data comparison, but Table A 5, Table A 6, and Table A 7 show the results of the uncertainty in the laminar flame speed for the experiments performed in this study.

4.3 Chemical Kinetics Modeling

The detailed chemical kinetics mechanism utilized in this work is under constant development and optimization at the Combustion Chemistry Centre and is available online at http://c3.nuigalway.ie/. The $H_2/CO/O_2$ mechanism is based on the work of Ó Conaire et al. (2004) with several significant updates based on recent experimental and kinetic data. The changes are partially described in Kéromnès et al. (2011) and will be fully detailed in an upcoming publication (Kéromnès et al., 2012). Flame speed simulations were performed with the Premix module of Chemkin Pro 15101 using the multi-component transport equations. Solutions were converged to approximately 1,000 grid points to provide grid-independent solutions. Kinetic, thermodynamic, and transport data utilized in this work are provided in the Appendix.

CHAPTER V

EXPERIMENT AND RESULTS

This study investigated how the laminar flame speed is affected over conditions that are relevant to syngas fuel blends. Ideally, the experiments should be conducted over as wide a range as possible of equivalence ratios (ϕ) for several syngas blends of H_2 and CO with varying levels of steam (0 – 15% by volume), initial pressure (1 – 10 atm), and initial temperature (323 – 423 K). The desired experimental conditions derived from these parameters are highly uncommon based on the available literature, lending to the significance of the experimental results presented herein. A DOE methodology was determined as the most efficient way to explore the entire range of variables shown in Table 5. Each factor was given three levels to provide greater detail over the range. Conditions relevant to gas turbine operating conditions set the overall ranges of the factors, while the specific levels were selected with the capabilities of the experimental facility as constraints. Some consideration was also given to ensure overlap with available data from the literature, for comparison.

Table 5 Four variables, each with three corresponding levels for the syngas experiments herein. The water dilution is on a percent of the total fuel mixture, including the H_2O.

Variable	***Level (1,2,3)***
Temperature (K)	323, 373, 423
Pressure (atm)	1, 5, 10
H_2O Dilution (% mole)	0, 7.5, 15
Syngas Comp. (H_2:CO)	5:95, 50:50, 100:0

A full-factorial matrix would require an overwhelming number of experiments (i.e., 81 combinations with about 10 tests for each). A DOE approach would significantly reduce the required number of conditions while still covering the desired parameter space. To this end, a Taguchi L9 matrix shown in Table 6 was applied to the four factors, reducing the number of conditions to a total of nine (Ross, 1996). This reduced matrix still allows for a comprehensive study over the entire range of parameters from fuel-lean to fuel-

rich conditions without compromising the significance of the results. Applying the nomenclature of Table 6 to the factor levels in Table 5 provides the appropriate combinations for each factor and establishes the target test matrix listed as Table 7. The steam dilution is defined as the molar percentage of the fuel mixture, $\chi = [X_{H2O}/(X_{H2}+X_{CO}+X_{H2O})]\times 100\%$, and "X" denotes the mole fraction for each species in the fuel mixture. All nine conditions shown in the test matrix were tested over a full excursion of fuel-to-oxidizer equivalence ratios (~0.8-5.0) to obtain the experimental flame speed envelope.

Table 6 Standard L9 DOE test matrix for four factors (*A*-*D*) at three levels (*1*-*3*) (Ross, 1996).

Experiment	***A***	***B***	***C***	***D***
1	1	1	1	1
2	1	2	2	2
3	1	3	3	3
4	2	1	2	3
5	2	2	3	1
6	2	3	1	2
7	3	1	3	2
8	3	2	1	3
9	3	3	2	1

Table 7 Laminar flame speed matrix with 9 blends using four factors (Temperature (*T*), Pressure (*P*), Steam Dilution (χ), and Syngas Composition (H_2:*CO*)) at three levels.

Exp.	***T (K)***	***P (atm)***	***χ (% by mole)***	***H_2:CO***
1	323	1	7.5	5:95
2	323	5	0	50:50
3*	323	1	15	100:0
4	373	1	0	100:0
5	373	5	15	5:95
6	373	10	7.5	50:50
7	423	1	15	50:50
8	423	5	7.5	100:0
9	423	10	0	5:95

*Pressure should be 10 atm but changed to 1 atm due to high steam concentration

5.1 Laminar Flame Speed at 323 K

For an initial preheat temperature of 323 K, Figure 26 shows new laminar flame speed experimental data for the three syngas mixtures with different dilutions of steam at initial pressures of 1 and 5 atm (i.e., experiments 1, 2, and 3 in Table 7). From an equivalence ratio over the range of about 0.5 to 5.0, a distinct trend can be noticed where the peak flame speed shifts to the fuel-rich end due mostly to the increased

concentration of carbon monoxide. Typically, an increase in the initial pressure will shift the peak flame speed to the left (Lowry et al., 2011), while an increase in carbon monoxide content will shift the peak to the right and broaden the flame speed "dome". The broadening of the flame speed "dome" physically represents the laminar flame speed becoming less influenced by the equivalence ratio, also shown in Sun et al. (2007). The addition of steam plays only a small role in adjusting the peak flame speed at different equivalence ratios; rather, it slows the chemical kinetics of the combustible mixtures and decreases the flame speed.

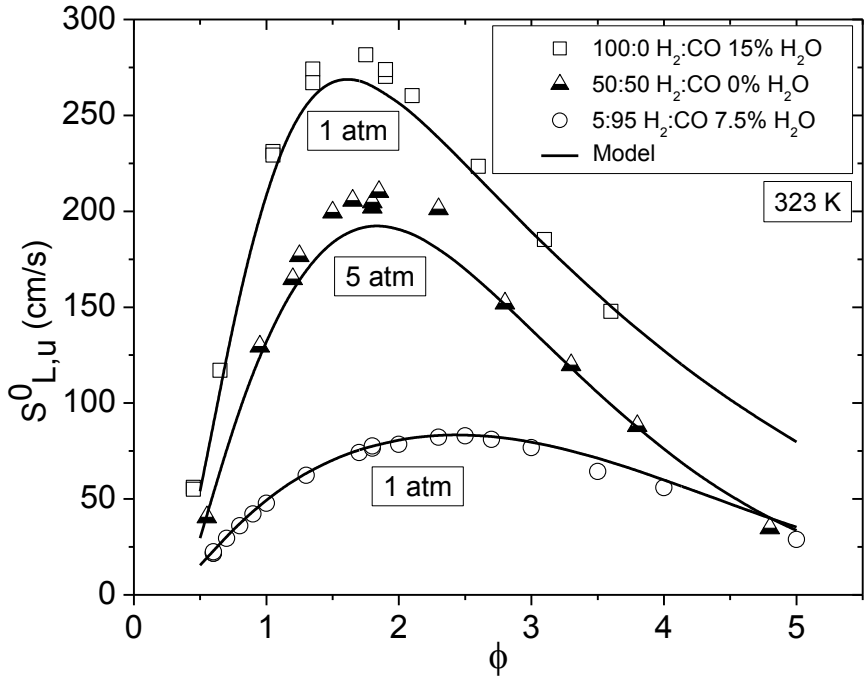

Figure 26 Laminar flame speed for the three syngas compositions at 1 and 5 atm each at different steam dilutions initially heated to 323 K compared to the chemical kinetics model (Exps. 1, 2, and 3 in Table 7).

5.2 Laminar Flame Speed at 373 K

Figure 27 shows the laminar flame speed results for the middle initial temperature, 373 K (experiments 4, 5, and 6 in Table 7). It can be seen how pressure appears to strongly influence the shift of the peak flame speed. The equivalence ratio at which the peak flame speed of the atmospheric, pure hydrogen mixture is

nearly the same as the 5-atm, 5:95 H_2:CO mixture; while in Figure 26, the peak shifts about a 0.8 difference in equivalence ratio between the pure hydrogen and 5:95 H_2:CO atmospheric experiments.

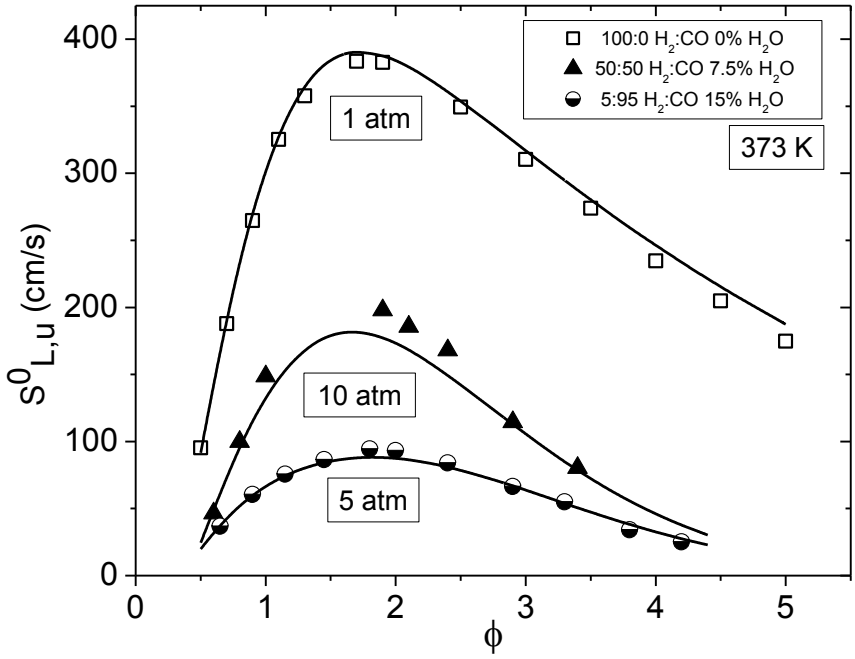

Figure 27 Laminar flame speed for three syngas compositions at 1, 5, and 10 atm each at different steam dilutions initially heated to 373 K compared to the chemical kinetics model (Exps. 4, 5, and 6 in Table 7).

5.3 Laminar Flame Speed at 423 K

How the laminar flame speed changes at an initial temperature of 423 K for the final three DOE conditions (experiments 7, 8, and 9 in Table 7) is shown in Figure 28. The continual broadening of the flame speed "dome" is still apparent with increasing CO concentration at this elevated temperature. Also, it is demonstrated that the initial temperature of the mixture appears to have a stronger influence on the flame speed than the steam dilution percentages. This result derives from the fact that the peak flame speed of the 5-atm, pure hydrogen mixture diluted with 7.5% steam at 423 K is about 465 cm/s; while the peak flame speed of the 1-atm, pure hydrogen mixture with 0% steam dilution at 373 K is about 380 cm/s.

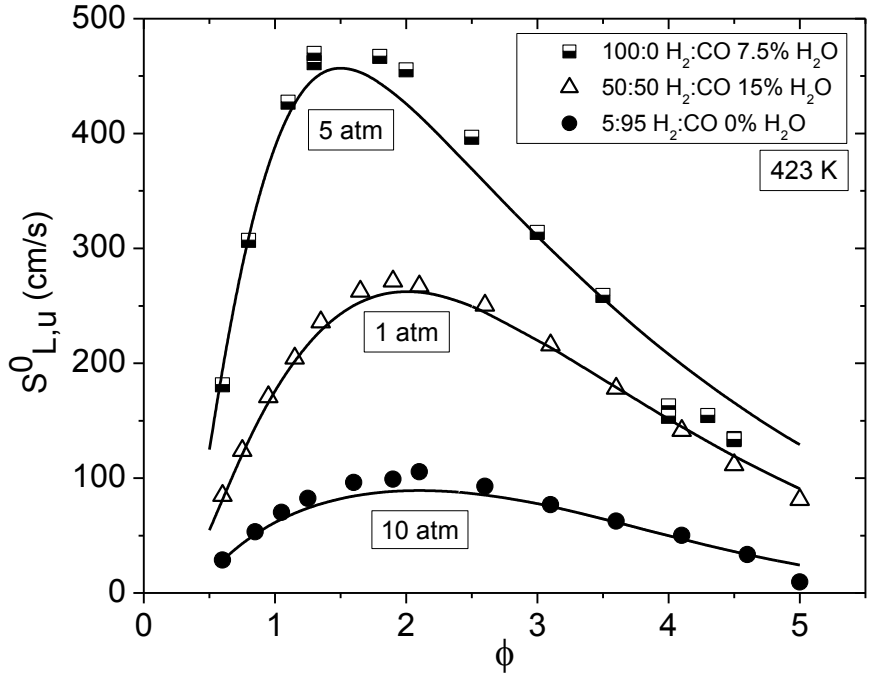

Figure 28 Laminar flame speed for three syngas compositions at 1, 5, and 10 atm each at different steam dilutions initially heated to 423 K compared to the kinetics model (Exps. 7, 8, and 9 in Table 7).

CHAPTER VI

DISCUSSION

6.1 Design of Experiments Analysis

The DOE approach provides the capability to demonstrate the most influential factor(s) on the experiment. By following the parameter analysis outlined in Ross (1996), a performance sensitivity calculation was done for the laminar flame speed, mass burning flux, and the Markstein length. The mass burning flux, m^0, is equal to the laminar flame speed times the un-burned density. This parameter is a more direct representation of the rate of the overall chemical reaction (Egolfopoulos and Law, 1990). The performance sensitivity calculation for each factor and equivalence ratio is the maximum difference between the averaged parameter values (i.e. laminar flame speed) at each DOE level (i.e. 1, 2, or 3). Table 8, Table 9, and Table 10 show the results of the sensitivity analysis for the mixtures studied in the DOE matrix for four oxygen equivalence ratios, φ_Ω, from fuel lean to fuel rich.

The oxygen-equivalence ratio modifies the normal equivalence ratio to account for the effect when fuel molecules contain oxidizer elements or oxidizer molecules contain fuel elements. This ratio is defined as the amount of oxygen atoms required to convert all the C and H atoms in the fuel-oxidizer mixture for stoichiometric combustion divided by the number of oxygen atoms present in the fuel-oxidizer mixture (Mueller, 2005). For the mixtures studied in this thesis, the oxygen equivalence ratio is related to the traditional equivalence ratio, φ, and the mole fraction of carbon monoxide, X_{CO}, by the following equation.

$$\varphi_\Omega = \frac{(1+X_{CO})}{\left(X_{CO}+\frac{1}{\varphi}\right)} \tag{18}$$

The oxygen equivalence ratio and the performance sensitivity analysis are used in the following sections to develop a meaningful discussion of how a DOE approach can provide insight into how temperature, pressure, water dilution, and syngas composition affect the laminar flame speed, mass burning flux, and the Markstein length.

Table 8 Laminar flame speed performance sensitivity analysis based on the maximum difference between the averaged laminar flame speeds at each DOE level (1, 2, or 3) for four oxygen equivalence ratios.

ϕ_Ω	T (K)	P (atm)	χ (% by mole)	H_2:CO
0.7	0.18	0.13	0.07	0.47
1	0.23	0.13	0.13	0.72
1.3	0.28	0.20	0.12	0.83
1.6	0.26	0.20	0.11	1.00

Table 9 Laminar mass burning flux performance sensitivity analysis based on the maximum difference between the averaged laminar mass burning fluxes at each DOE level (1, 2, or 3) for four oxygen equivalence ratios.

ϕ_Ω	T (K)	P (atm)	χ (% by mole)	H_2:CO
0.7	0.26	0.18	0.22	0.41
1	0.39	0.66	0.60	0.51
1.3	0.61	1.00	0.77	0.67
1.6	0.57	0.82	0.61	0.97

Table 10 Markstein length performance sensitivity analysis based on the maximum difference between the averaged Markstein lengths at each DOE level (1, 2, or 3) for four oxygen equivalence ratios.

ϕ_Ω	T (K)	P (atm)	χ (% by mole)	H_2:CO
0.7	0.27	0.43	0.31	1.00
1	0.10	0.07	0.15	0.19
1.3	0.04	0.20	0.08	0.04
1.6	0.18	0.13	0.21	0.34

6.2 Water Dilution Effect

Based on the excellent behavior of the model when compared to the experimental data over the comprehensive range of conditions explored herein, the model can be used with confidence to study further the impact of water dilution on the laminar flame speed of syngas mixtures. Two mixtures featuring extreme H_2:CO dilutions were used to calculate laminar flame speed values at an equivalence

ratio of 0.5, which is of relevance to the gas turbine industry. Figure 29 and Figure 30 show the flame speed versus percent water dilution at 323 and 423 K, respectively. For mixtures with higher concentrations of CO (i.e., 5:95 H_2:CO), the water concentration has only a small effect on the laminar flame speed; a slight increase in flame speed is seen for higher moisture concentrations at both of these temperatures at 1 atm and a subtle decrease in flame speed at 10 atm. As the concentration of CO in the fuel blend is reduced (i.e., 95:5 H_2:CO), the water has a much larger effect on the laminar flame speed; in fact, the presence of steam has a negative effect on the flame speed. These results are similar to the trends presented by Das et al. (2011).

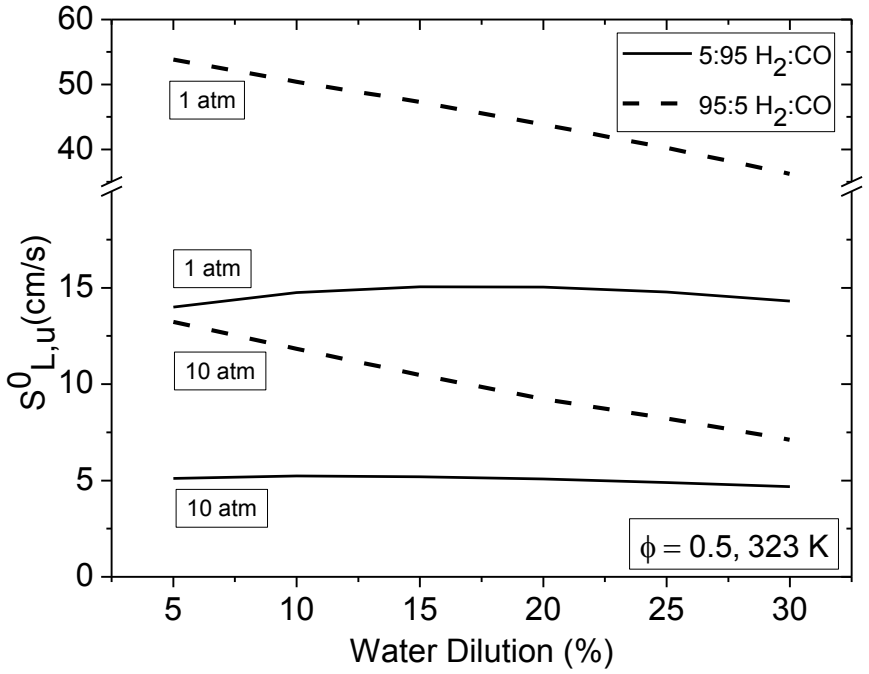

Figure 29. Effect of water dilution on the laminar flame speed for 5:95 H_2:CO and 95:5 H_2:CO with air mixtures at 323 K and $\phi = 0.5$.

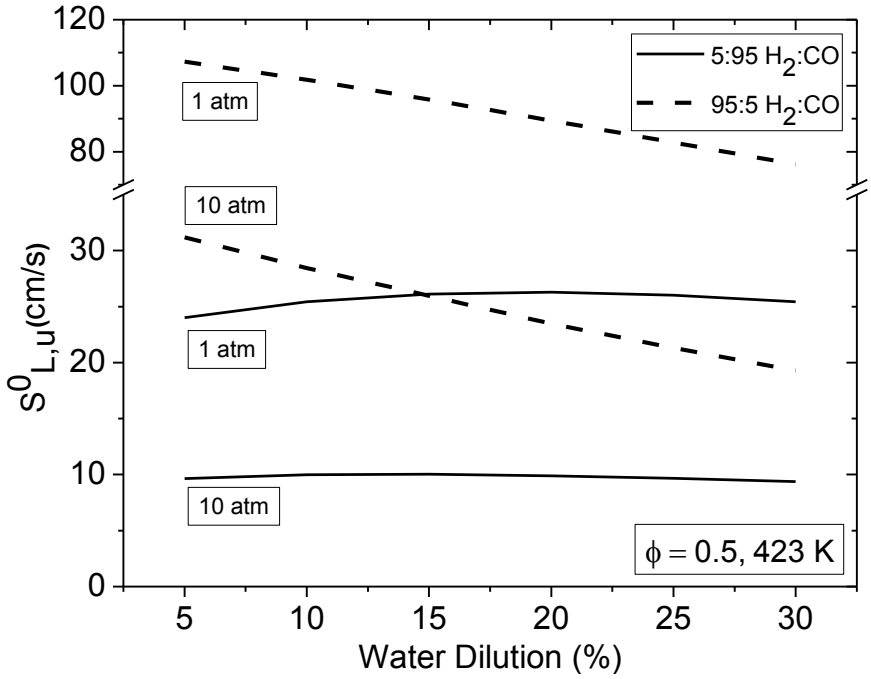

Figure 30. Effect of water dilution on the laminar flame speed for 5:95 H_2:CO and 95:5 H_2:CO with air mixtures at 423 K and $\phi = 0.5$.

6.3 Laminar Flame Speed Comparison

The experiments performed at an initial pressure of 1 atm, shown in Figure 31, demonstrate how steam dilution, carbon monoxide concentration, and temperature change the chemical kinetics. As mentioned earlier, an increase in CO concentration appears to shift the peak flame speed towards the fuel-rich side; while it appears that the amount of steam dilution has little or no effect on shifting the flame speed to richer equivalence ratios, as seen by the pure-hydrogen case at 323 K and the 50:50 H_2:CO case at 423 K, both diluted with the same amount of steam. These two mixtures also appear to show the strong influence temperature has on the flame speed with the flame speed values being nearly the same. However, if the definition of the oxygen equivalence ratio is implemented and the performance sensitivity of the flame speed is displayed as a column chart, as shown in Figure 32, the adjusted trends of the laminar flame speed from the atmospheric mixtures, shown in Figure 33, can be explained.

The apparent shift in peak flame speeds are adjusted to occur near the same equivalence ratio with changing the equivalence ratio from the traditional definition to the definition based on the number of oxygen atoms. This change is appropriate because the equivalence ratio is supposed to describe the proximity of the reactant mixture to its stoichiometric condition. When a reactant mixture contains fuel molecules with oxidizer elements (i.e. syngas), the oxidizer elements must be accounted for as an oxidizer instead of being lumped in as part of the fuel component, as is done with the traditional equivalence ratio. Mueller (2005) explains in further detail why and how the oxygen equivalence ratio accurately quantifies the mixture stoichiometry.

Figure 32 shows the amount of carbon monoxide dilution has a strong influence on the laminar flame speed from fuel lean to fuel rich. More importantly, the carbon monoxide dilution has an increasing impact on the flame speed beyond the stoichiometric condition. When the fuel mixture is lean and all of the fuel is consumed, the initial temperature has an important role on the effect on the flame speed where the flame speeds of the 100:0 H_2:CO mixture at 373K are nearly the same as the 50:50 H_2:CO mixture at 423K. However, as there becomes increasingly more excess fuel in the products, the influence of the amount of carbon monoxide dilution strongly impacts the laminar flame speed. This effect can also be shown by looking at the adiabatic flame temperatures of the mixtures as a function of the oxygen equivalence ratio, shown in Figure 34. At an equivalence ratio of 2, the difference in the adiabatic flame temperature is about 575 K, while the change in the adiabatic flame temperature at an equivalence ratio of 1 is only about 125 K. The laminar flame speed is related to the adiabatic flame temperature, T_{ad}, the un-burned density, ρ_u, and the activation temperature, T_a, by the following equation (Law, 2006).

$$S_{L,u}^0 \sim \frac{T_{ad}^2}{\rho_u} \, e^{-T_a/2T_{ad}} \tag{19}$$

The adiabatic flame temperature, controlled by the heat of combustion of the fuel, has a dominant influence on the laminar flame speed. The DOE performance sensitivity analysis is able to capture the major effects that control the trends of the laminar flame speed of the mixtures performed herein.

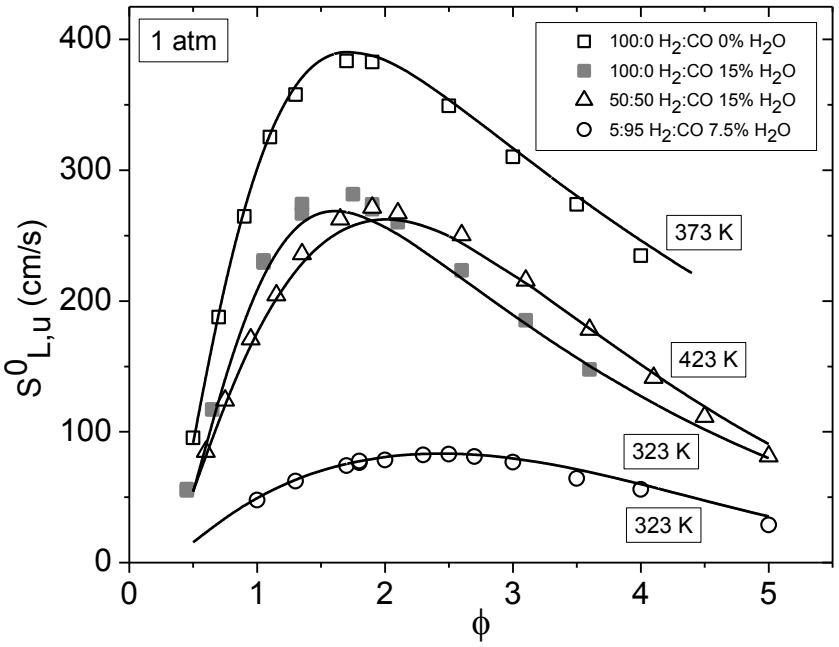

Figure 31 Laminar flame speed comparison of atmospheric-pressure mixtures (Exps. 1, 3, 4, and 7 in Table 7). The chemical kintics model is shown as the solid lines. The flame speed can vary by a factor of 4 due to the variations in water content, initial temperature, and H_2:CO split considered herein.

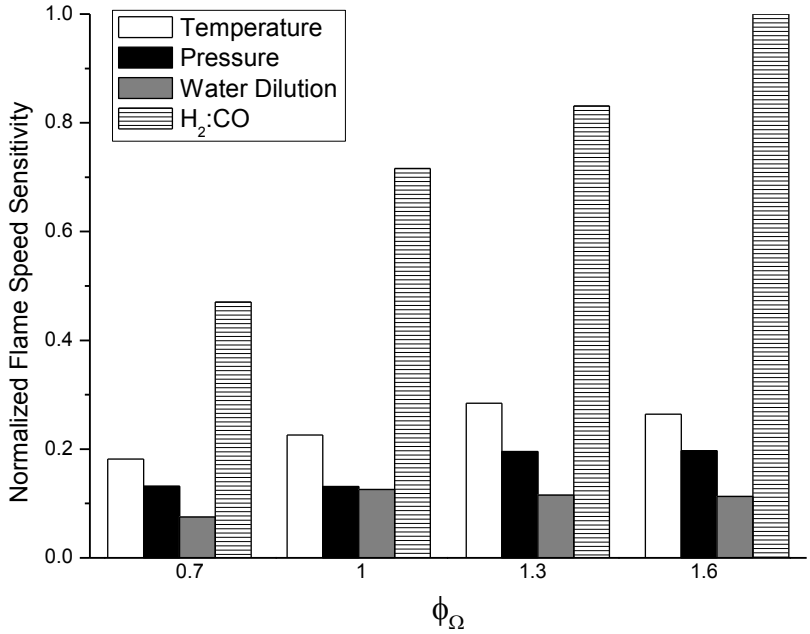

Figure 32 Normalized flame speed sensitivity between the four factors studied (temperature, pressure, water dilution, and H_2:CO) at four oxygen equivalence ratios from fuel-lean to fuel-rich.

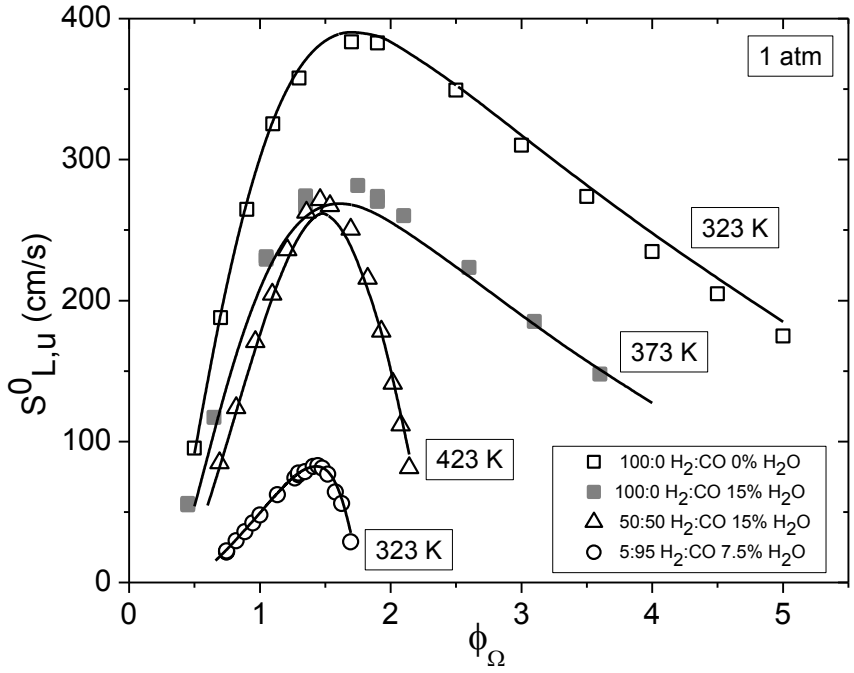

Figure 33 Laminar flame speed comparison of the atmospheric-pressure mixtures (Exps. 1, 3, 4, and 7 in Table 7). The solid lines represent the chemical kinetics model.

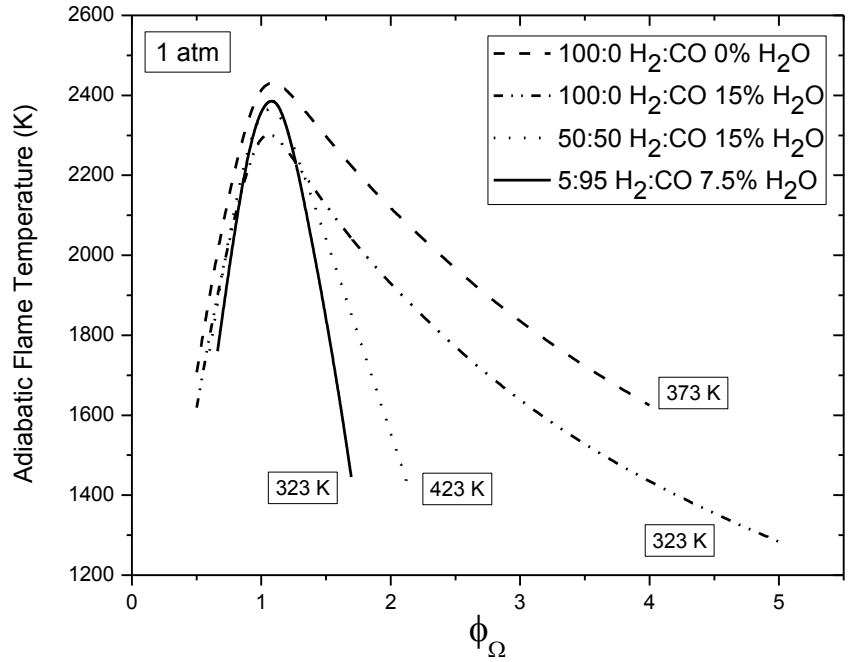

Figure 34 Adiabatic flame temperature comparison of the atmospheric-pressure mixtures (Exps. 1, 3, 4, and 7 in Table 7).

6.4 Laminar Mass Burning Flux Comparison

Figure 35 shows the performance sensitivity analysis for the mass burning flux as a function the oxygen equivalence ratio. There is no clear trend that can be interpreted in the plot except that the hydrogen and carbon monoxide ratio continues to have a strong influence for fuel lean conditions. As the equivalence ratio approaches stoichiometric and beyond, several factors appear to be competing against one another, impacting the mass burning flux. Measuring the mass burning flux is not an appropriate way to display the results of a DOE method because several factors can affect the mass burning flux. However, since the mass burning flux is equivalent to the product of the un-burned density and the laminar flame speed, the mass burning flux is expected to have a similar trend as the laminar flame speed for the atmospheric mixtures (Figure 33). Figure 36 confirms that the trend of the mass burning flux as a function of the oxygen equivalence ratio is similar to the laminar flame speed trend.

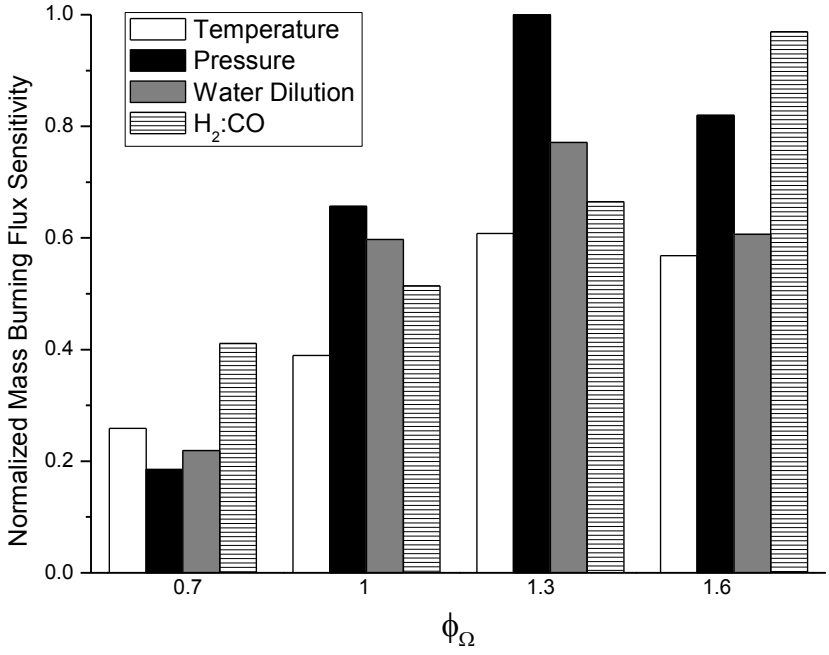

Figure 35 Normalized mass burning flux sensitivity between the four factors studied (temperature, pressure, water dilution, and H_2:CO) at four oxygen equivalence ratios from fuel-lean to fuel-rich.

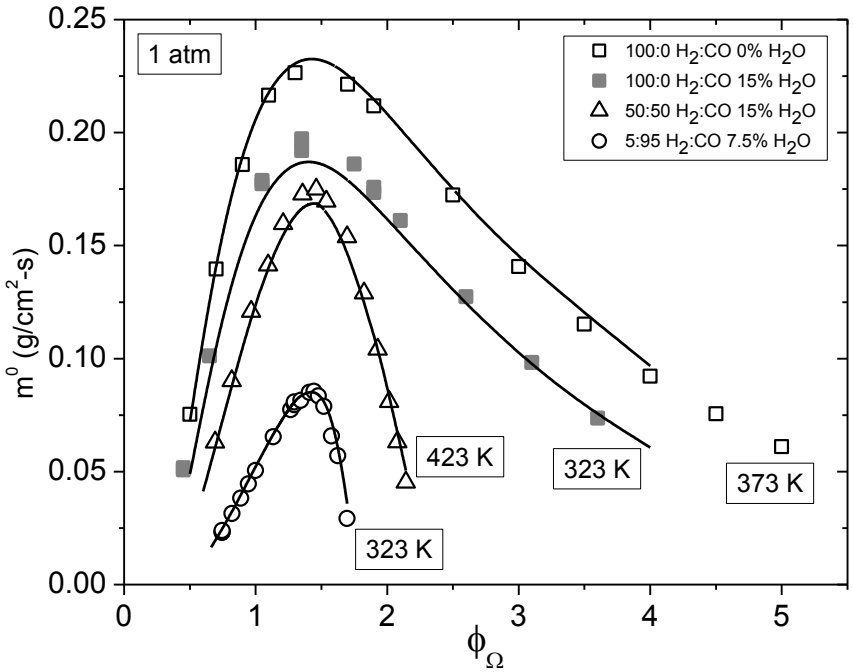

Figure 36 Comparison of the mass burning flux of the atmospheric-pressure mixtures (Exps. 1, 3, 4, and 7 in Table 7). The solid lines represent the chemical kinetics model.

6.5 Markstein Length Comparison

One method to show how combustible mixtures are sensitive to flame stretch is to look at the Markstein length trends. If the Markstein length is negative, the flame front is affected by thermal-diffusional instabilities and will have irregular distortions. A positive Markstein length will be free of thermal-diffusional instabilities but may still be affected by hydrodynamic instabilities. The performance sensitivity analysis of the Markstein length, shown in Figure 37, demonstrates that the thermal-diffusional behavior of the fuel mixture (H_2:CO ratio) dominates on the fuel lean side of the mixtures studied in this thesis. However, as the equivalence ratio increases, there is no dominating factor. This trend is supported by displaying the Markstein lengths for the 1-atm experimental data in Figure 38. The lines in Figure 38 are shown to help guide the eye for each experiment. The dominance of the H_2:CO ratio can be seen on the fuel lean side by comparing the Markstein lengths of the 5:95 H_2:CO mixture to the other mixtures. Then the Markstein lengths for all the mixtures oscillate around the same value from stoichiometric to about an oxygen equivalence ratio of 1.5 demonstrating the competing nature of the four factors. For oxygen

equivalence ratios beyond 1.5, the amount of CO dilution appears to have a strong influence, but it is clear from Figure 37 that other factors may be influencing the hydrodynamic effects of the mixtures.

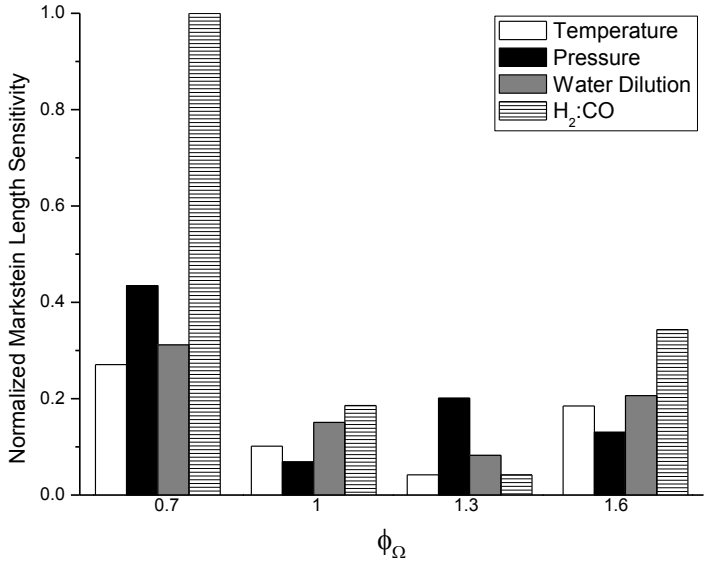

Figure 37 Normalized Markstein length sensitivity between the four factors studied (temperature, pressure, water dilution, and H_2:CO) at four oxygen equivalence ratios from fuel-lean to fuel-rich.

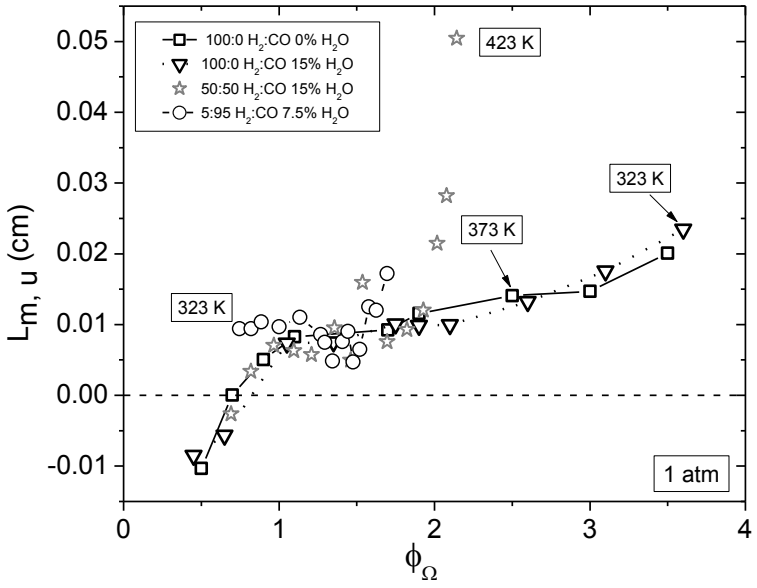

Figure 38 Measured Markstein lengths for the atmospheric-pressure mixtures (Exps. 1, 3, 4, and 7 in Table 7). The lines shown are to guide the eye for the trend of each data set.

6.6 Sensitivity Analysis

A reaction rate sensitivity analysis was performed by associated colleagues at the National University at Galway Ireland using Chemkin Pro 15101 to explain the kinetic effect of water dilution depicted in Figure 29 and Figure 30. The analysis was performed on the atmospheric mixtures shown in Figure 29 at zero and 15% water dilution as described in Table 11. Prior to analyzing the sensitivity results, it is necessary to decouple the thermal and chemical effects of water dilution. This separation was performed by diluting the mixture with a 'dummy' species (with identical thermochemistry as water) instead of water, thus reproducing the thermal effect of water, while excluding any chemical interactions. Figure 39 and Figure 40 depict the sensitivity analysis results at a low-CO and a high-CO condition, respectively.

Table 11 Condition at which sensitivity analysis was performed.

	H_2	CO	O_2	H_2O	N_2	ϕ	P (atm)	T (K)	%H_2O of Fuel
MIX A	0.4750	0.0250	0.5000	0.0000	1.8800	0.5	1.0	323.0	0.0
MIX B	0.4038	0.0213	0.4250	0.0750	1.5980	0.5	1.0	323.0	15.0
MIX C	0.0250	0.4750	0.5000	0.0000	1.8800	0.5	1.0	323.0	0.0
MIX D	0.0213	0.4038	0.4250	0.0750	1.5980	0.5	1.0	323.0	15.0

At the low-CO condition, a 15% water dilution causes a 16% reduction in predicted flame speed. The thermal effect of water dilution dominates this reduction, contributing approximately 75% of the reduction. The remaining 25% can be attributed to chemical effects. At the low-CO concentrations, the flame speed is most sensitive to the reaction $H_2+OH \rightleftarrows H_2O+H$, which has a large promoting effect. The most inhibiting reaction is the collisional stabilized formation of hydroperoxy radical via $H+O_2(+M) \rightleftarrows HO_2(+M)$. The large collisional efficiency is associated with water, which will increase the rate of this reaction and thus reduce the flame speed.

At the high-CO condition, the chemical effect of water dilution is more pronounced. The chemical reactivity overcomes the thermal effect causing an overall increase in reactivity and a subsequent faster flame speed. The sensitivity analysis reveals that carbon monoxide chemistry is dominant at this condition

with the reaction CO+OH⇄CO_2+H having a very pronounced promoting effect. The increase in reactivity in the water-diluted case can be attributed to the increased sensitivity of the reaction H_2O+O⇄OH+OH, producing two hydroxide radicals, which are free to react further with CO. This effect was also noted by Das et al. (2011).

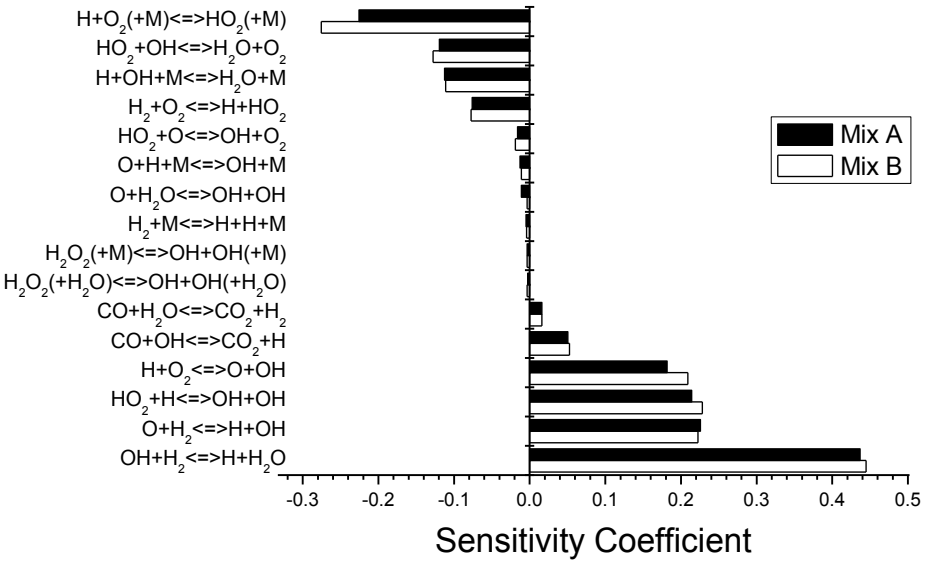

Figure 39 Reaction rate sensitivity analysis at low CO concentration of atmospheric mixtures. Mix A is composed of 95:5 H_2:CO diluted with 0% H_2O at ϕ = 0.5 and 323 K while mix B is composed of 95:5 H_2:CO diluted with 15% H_2O at ϕ = 0.5 and 323 K.

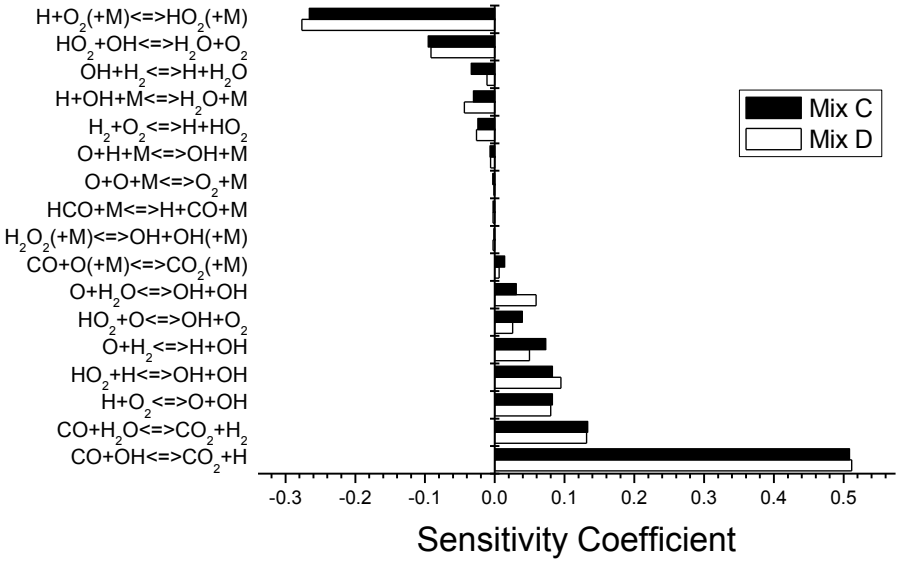

Figure 40 Reaction rate sensitivity analysis at high CO concentration of atmospheric mixtures. Mix C is composed of 5:95 H_2:CO diluted with 0% H_2O at ϕ = 0.5 and 323 K while mix D is composed of 5:95 H_2:CO diluted with 15% H_2O at ϕ = 0.5 and 323 K.

CHAPTER VII

CONCLUSIONS

This thesis presents new experimental data for three syngas fuels with varying steam dilution at several initial temperatures and pressures. A Design of Experiments (DOE) methodology allowed the authors to explore the combination of four different factors with three levels. The three syngas blends studied were 100:0 H_2:CO, 50:50 H_2:CO, 5:95 H_2:CO at initial pressures of 1, 5, and 10 atm. The other factors included initial temperatures of 323, 373, and 473 K; and steam dilutions of 0, 7.5, and 15% on a molar basis of the fuel blend. To perform these experiments at the declared conditions, a new high-temperature and high-pressure cylindrical vessel was developed. This vessel was designed to perform initial temperatures and pressures up to 600 K and 30 atm, respectively. Several validation experimental studies where performed on the HTHP vessel before studying the syngas blend set of experiments including temperature uniformity, hydrogen mixture experiments at elevated pressure and temperature, syngas mixture experiments at elevated pressures, and syngas diluted with water. All experimental series showed good agreement with previously published data and the chemical kinetics model.

Some of the DOE experimental data are compared to published data demonstrating good agreement, while all new data are compared to the most recent, improved chemical kinetics model. Several DOE performance sensitivity analyses were done to show the dominating factor or factors on the laminar flame speed, mass burning flux, and Markstein length. The laminar flame speed was the only measured result that showed a clear trend of dominance from the H_2:CO ratio. The mass burning flux and the Markstein length require further in-depth analysis to understand the impact of each factor. However, the Markstein length did appear to be influenced by the amount of carbon monoxide dilution. The overall agreement with the model is excellent in most cases with some discrepancies seen around the peak flame speed for particular mixtures, which identifies potential areas where improvements can be made.

REFERENCES

Aldredge, R.C., and Killingsworth, N.J. 2004. Experimental evaluations of Markstein-number influence on thermoacoustic instability. *Combustion and Flame*, **137**, 178-197.

American Society of Mechanical Engineers. 2000. *ASME Boiler and Pressure Vessel Code, Section II and VIII.*

Aung, K.T., Hassan, M.I., and Faeth, G.M. 1997. Flame stretch interactions of laminar premixed hydrogen/air flames at normal temperature and pressure. *Combustion and Flame*, **109**, 1-24.

Bourque, G., Healy, D., Curran, H., Zinner, C., Kalitan, D., de Vries, J., Aul, C., and Petersen, E. 2008. Ignition and flame speed kinetics of two natural gas blends with higher levels of hydrocarbons. 2008 ASME Turbo Expo, Berlin, Germany, June 9-13, Paper # GT2008-41344.

Bouvet N., Chauveau C., Gokalp I., and Halter F. 2011. Experimental studies of the fundamental flame speeds of syngas (H_2/CO)/air mixtures. *Proceedings of the Combustion Institute*, **33**, 913-920.

Brown, M.J., McLean, I.C., Smith, D.B., and Taylor, S.C. 1996. Markstein lengths of CO/H_2/air flames, using expanding spherical flames. *Proceedings of the Combustion Institute*, **26**, 875-881.

Burke M. P., Chaos M., Dryer F. L., and Ju Y. 2010. Negative pressure dependence of mass burning rates of H_2/CO/O_2/diluent flames at low flame temperature. *Combustion and Flame*, **157**, 618-631.

Burke M. P., Chen Z., Ju Y., and Dryer F. L. 2009. Effect of cylindrical confinement on the determination of laminar flame speeds using outwardly propagating flames. *Combustion and Flame*, **156**, 771-779.

Burke M. P., Qin X., Ju Y., and Dryer F. L. 2007. Measurements of hydrogen syngas flame speeds at elevated pressures. *5th U.S. Combustion Meeting*, Paper No. A16.

Chacartegui R., Sanchez D., Munoz de Escalona J.M., Jimenez-Espadafor F. Munoz A., and Sanchez T. 2011. SPHERA project: Assessing the use of syngas fuels in gas turbines and combined cycles from a global perspective. *Fuel Processing Technology*, Available online 26 November 2011, ISSN 0378-3820, 10.1016/j.fuproc.2011.11.004.

CHEMKIN-PRO 15101. (2010). Reaction Design, San Diego, CA.

Chernov, N. 2010. *Circular and Linear Regression: Fitting circles and lines by least squares*. CRC Press, Boca Raton, FL 33487-2742.

Choas M. and Dryer F. L. 2008. Syngas combustion kinetics and applications. *Combustion Science and Technology*, **180**, 1053-1096.

Dahoe A. E. 2005. Laminar burning velocities of hydrogen-air mixtures from closed vessel gas explosions. *Journal of Loss Prevention in the Process Industries*, **18**, 152-166.

Das A. K., Kumar K., and Sung C.-J. 2011. Laminar flame speeds of moist syngas mixtures. *Combustion and Flame*, 158, 345-353.

de Vries, J. 2009. A study on spherically expanding flame speeds of methane, ethane, and methane/ethane mixtures at elevated pressures. Doctoral Dissertation, Texas A&M University, College Station, TX, USA.

de Vries, J., Lowry, W.B., Serinyel, Z., Curran, H.J., and Petersen, E.L. 2010. Laminar flame speed measurements of dimethyl ether in air at pressures up to 10 atm. *Fuel*, **90**, 331-338.

Dong C., Zhou Q., Zhao Q., Zhang Y., Xu T., and Hui S. 2009. Experimental study on the laminar flame speed of hydrogen/carbon monoxide/air mixtures. *Fuel*, **88**, 1858-1863.

Dowdy, D.R., Smith, D.B., Taylor, S.C., and Williams, A. 1990. The use of expanding spherical flames to determine burning velocities and stretch effects in hydrogen/air mixtures. *Proceedings of the Combustion Institute*, **23**, 325-332.

Egolfopoulos F. N. and Law C. K. 1990. An experimental and computational study of the burning rates of ultra-lean to moderately-rich H2/O2/N2 laminar flames with pressure variations. *Proceedings of the Combustion Institute*, 23, 333-340.

Hassan M. I., Aung K. T., and Faeth G. M. 1997. Properties of laminar premixed CO/H_2/Air flames at various pressures. *Journal of Propulsion and Power*, **13**, 239-245.

Hu E., Huang Z., He J., Miao H. 2009. Experimental and numerical study on laminar burning velocities and flame instabilities of hydrogen-air mixtures at elevated pressures and temperatures. *International Journal of Hydrogen Energy*, 34, 8741-8755.

Kéromnès, A., Metcalfe, W. K., Donohoe, N., Curran, H. J., Pitz W. J. 21-23/03/2011. Detailed chemical kinetic model for H2 and H2/CO (syngas) mixtures at elevated pressure. 7th US Nat. Meeting of the Comb. Inst, Atlanta.

Kéromnès A., Metcalfe, W. K., Donohoe, N., Das, A. K., Sung, C. J., Mathieu, O., Krejci, M., Petersen, E. L., Pitz, W. J., and Curran, H. J. 2012. Detailed Chemical Kinetic Model for Hydrogen and Syngas Mixtures at Elevated Pressure. *Combustion and Flame*, in preparation.

Kuznetsov M., Redlinger R., Breitung W., Grune J., Friedrich A., and Ichikawa N. 2010. Laminar burning velocities of hydrogen-oxygen-steam mixtures at elevated temperatures and pressures. *Proceedings of the Combustion Institute*, 33, 895-903.

Kwon O. C. and Faeth G. M. 2001. Flame/stretch interactions of premixed hydrogen-fueled flames: measurements and predictions. *Combustion and Flame*, 124, 590-610.

Lamoureux N., Djebaili-Chaumeix N., and Paillard C. E. 2003. Laminar flame velocity determination for H_2-air-He-CO_2 mixtures using the spherical bomb method. *Experimental Thermal and Fluid Science*, 27, 385-393.

Law, C. K. 2006. *Combustion Physics*. Cambridge University Press, Cambridge, New York, 263-277.

Lieuwen, T.C. and Yang, V. 2005. *Combustion Instabilities in Gas Turbine Engines: Operational Experience, Fundamental Mechanisms, and Modeling*. AIAA, Danvers, MA, 2005.

Lowry, W.B., de Vries, J., Krejci, M., Petersen, E., Serinyel, Z., Metcalfe, W.K., Curran, H.J., and Bourque, G. 2011. Laminar flame speed measurements and modeling of pure alkanes and alkane blends at elevated pressures. *Journal of Engineering for Gas Turbines and Power*, **133**,

Markstein, G.H. 1964. *Non-Steady Flame Propagation*, Pergamon, New York.

McLean I. C., Smith D. B., and Taylor S.C. 1994. The use of carbon monoxide/hydrogen burning velocities to examine the rate of the CO + OH reaction. *Proceedings of the Combustion Institute*, **25**, 749-757.

Moffat, R. J. 1988. Describing uncertainties in experimental results. *Experimental Thermal and Fluid Science*, **1**, 3-17.

Mueller, C. J. 2005. The quantification of mixture stoichiometry when fuel molecules contain oxidizer elements or oxidizer molecules contain fuel elements. SAE Paper #2005-01-3705.

Natarajan J., Kochar Y., Lieuwen T., Seitzman J. 2009. Pressure and preheat dependence of laminar flame speeds of $H_2/CO/CO_2/O_2$/He mixtures. *Proceedings of the Combustion Institute*, **32**, 1261-1268.

Natarajan J., Nandula S., Lieuwen T., and Seitzman J. 2005. Laminar flame speeds of synthetic gas fuel mixtures. ASME Paper #GT2005-68917.

Ó Conaire, M., Curran, H. J., Simmie, J. M., Pitz, W. J., and Westbrook, C. K. 2004. A comprehensive modeling study of hydrogen oxidation. *International Journal of Chemical Kinetics*, **36**, 603-622.

Pareja J., Burbano H. J., and Ogami Y. 2010. Measurements of the laminar burning velocity of hydrogen-air premixed flames. *International Journal of Hydrogen Energy*, **35**, 1812-1818.

Prathap C., Ray A., and Ravi M. R. 2008. Investigation of nitrogen dilution effects on the laminar burning velocities and flame stability of syngas fuel at atmospheric condition. *Combustion and Flame*, **155**, 145-160.

Ross, P. J. 1996. *Taguchi techniques for quality engineering*. McGraw-Hill, New York, New York.

Rumminger, M. D. and Linteris, G.T. 2000. Inhibition of Premixed Carbon Monoxide–Hydrogen–Oxygen–Nitrogen Flames by Iron Pentacarbonyl. *Combustion and Flame*, **120**, 451-464.

Settles, G.S. 2006. *Schlieren and shadowgraph techniques: visualizing phenomena in transparent media*, Springer, Heidelberg, Germany.

Sun H., Yang S. I., Jomaas G., and Law C. K. 2007. High-pressures laminar flame speeds and kinetic modeling of carbon monoxide/hydrogen combustion. *Proceedings of the Combustion Institute*, **31**, 439-446.

Tse S.D., Zhu D. L., and Law C.K. 2000. Morphology and burning rates of expanding spherical flames in H_2/O_2/inert mixtures up to 60 atmospheres. *Proceedings of the Combustion Institute*, 28, 1793-1800.

Turns, S.R. 2000. *An Introduction to Combustion: Concepts and Applications*, 2nd ed., McGraw Hill, Boston, 253-283.

U.S. Department of Transportation. 2003. *Metallic Materials Properties Development and Standardization (MMPDS-01)*, 195-212.

Vagelopoulos C. M., Egolfopoulos F. N., and Law C. K. 1994. Further considerations on the determination of laminar flame speeds with the counterflow twin-flame technique. *Proceedings of the Combustion Institute*, 25, 1341-1347.

Verhelst S., Woolley R., Lawes M., and Sierens R. 2005. Laminar and unstable burning velocities and Markstein lengths of hydrogen-air mixtures at engine-like conditions. *Proceedings of the Combustion Institute*, 30, 209-216.

Williams, T. C. and Shaddix C. R. 2007. Contamination of carbon monoxide with metal carbonyl: Implications for combustion research. *Combustion Science and Technology*, **179**, 1225-1230.

Young, W., Budynas, R. 2002. *Roark's Formulas for Stress and Strain*, 7th-ed, McGraw-Hill Companies, Inc., 683.

APPENDIX

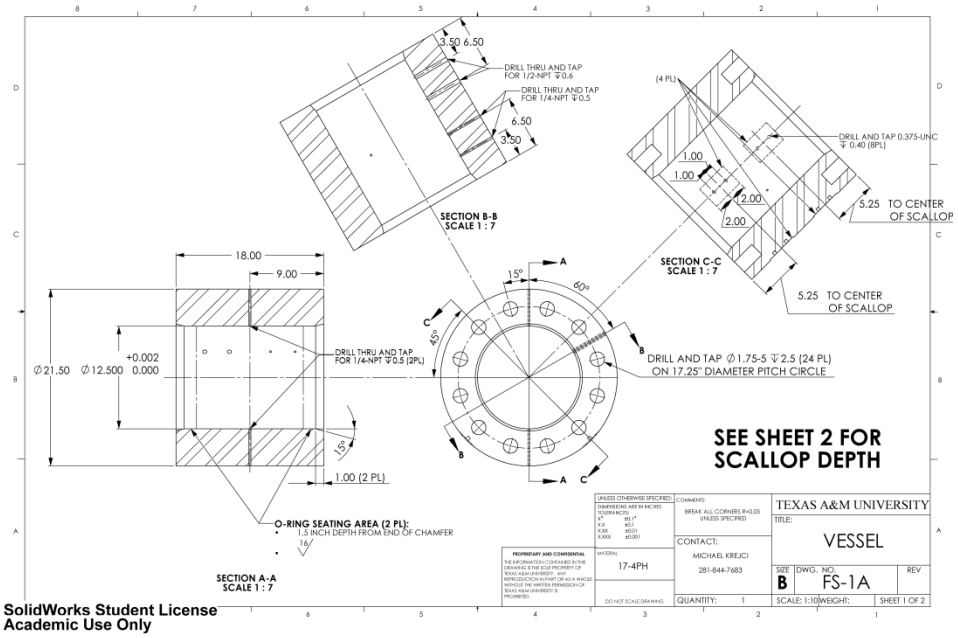

Figure A 1 Vessel body machine drawing, pg 1.

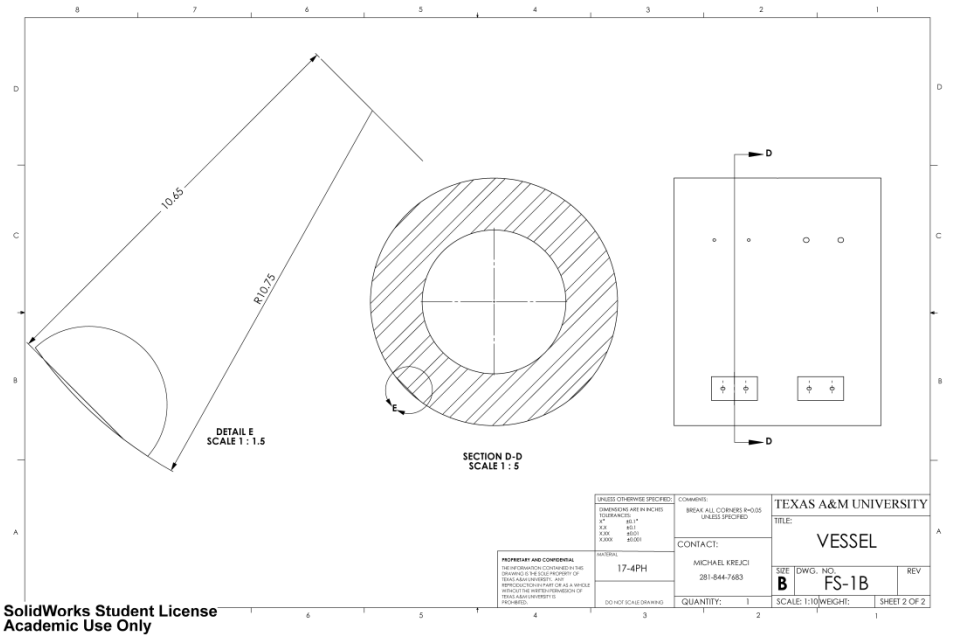

Figure A 2 Vessel body machine drawing, pg 2.

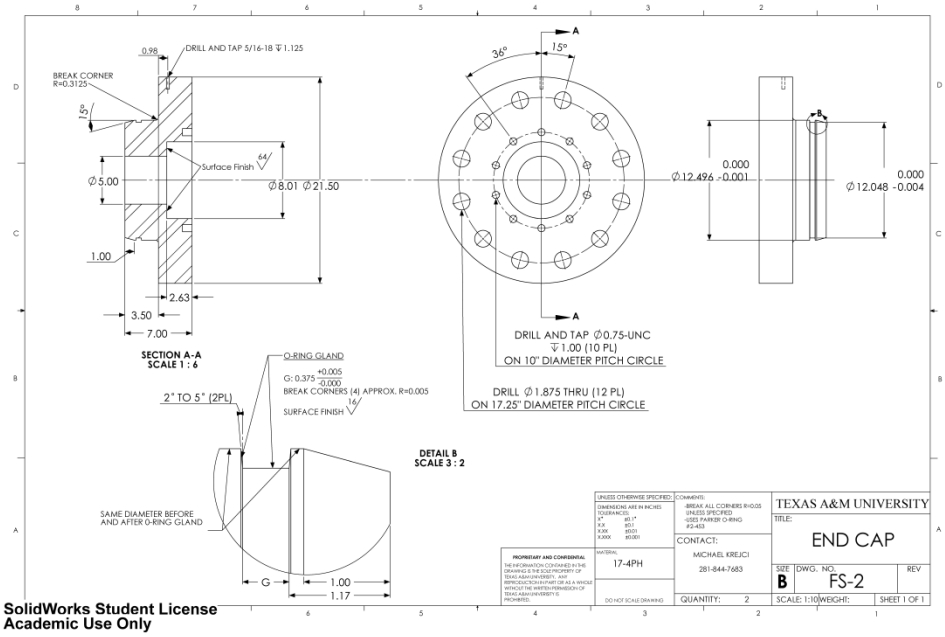

Figure A 3 End cap machine drawing.

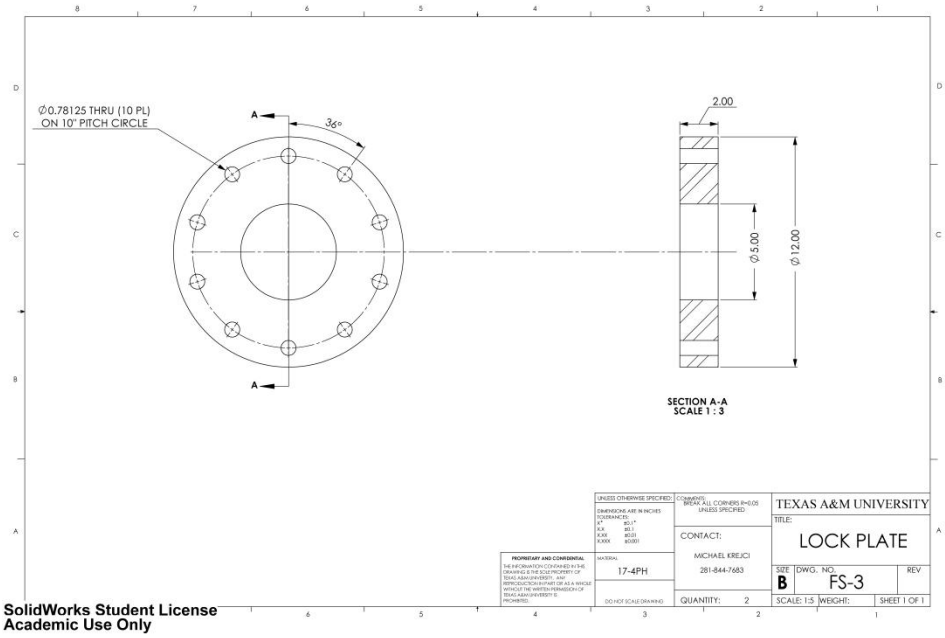

Figure A 4 Lock plate machine drawing.

Table A 1 Experimental data for atmospheric hydrogen-air at 298, 373, and 443 K.

ϕ	P_i (atm)	T_u (K)	σ	$S^0_{L,u}$ (cm/s)	L_m (cm)
0.5	1	295	5.041	64.7	-0.009
0.6	1	297	5.562	94.3	-0.006
0.7	1	298	6.012	124.4	-0.002
0.8	1	298	6.391	169.9	0.007
0.9	1	297	6.696	194.0	0.008
1.0	1	295	6.894	218.0	0.009
1.1	1	296	6.923	236.7	0.009
1.2	1	298	6.855	254.9	0.009
1.3	1	297	6.764	267.4	0.009
1.4	1	295	6.669	275.0	0.009
1.5	1	298	6.574	280.3	0.009
1.6	1	296	6.480	282.8	0.009
1.7	1	296	6.388	283.8	0.010
1.8	1	295	6.298	282.9	0.011
1.9	1	295	6.210	280.3	0.012
2.0	1	298	6.124	278.9	0.012
2.5	1	296	5.729	249.1	0.014
3.0	1	296	5.385	217.4	0.018
3.5	1	297	5.084	187.6	0.022
4.0	1	296	4.821	158.7	0.027
4.5	1	295	4.588	133.0	0.037
5.0	1	295	4.381	110.1	0.047
0.5	1	370	4.180	95.3	-0.010
0.7	1	373	4.938	187.8	0.000
0.9	1	373	5.459	264.8	0.005
1.1	1	373	5.635	325.3	0.008
1.3	1	372	5.524	357.8	0.007
1.7	1	370	5.237	383.5	0.009
1.9	1	371	5.099	382.8	0.012
2.5	1	374	4.725	349.3	0.014
3.0	1	372	4.456	310.3	0.015
3.5	1	373	4.220	273.9	0.020
4.0	1	372	4.013	234.8	0.020
4.5	1	373	3.831	204.7	0.025
5.0	1	373	3.668	174.9	0.032
0.5	1	444	3.639	141.2	-0.006
0.8	1	444	4.498	314.9	0.007
1.3	1	444	4.742	467.6	0.007
1.7	1	444	4.512	499.6	0.010
1.9	1	444	4.400	496.8	0.010
2.5	1	443	4.094	458.3	0.013
3.0	1	444	3.872	415.3	0.015
3.5	1	443	3.677	367.7	0.018
4.0	1	443	3.506	325.6	0.019

Table A 2 Experimental data for 5- and 10-atm hydrogen diluted with 1:7 O_2:He at 298, 373, and 443 K.

ϕ	P_i (atm)	T_u (K)	σ	$S^0_{L,u}$ (cm/s)	L_m (cm)
0.5	5	295	4.729	40.6	-0.003
0.8	5	299	6.258	186.4	0.005
1.0	5	298	6.960	245.3	0.005
1.2	5	297	6.823	278.7	0.003
1.5	5	297	6.482	300.5	0.004
1.7	5	296	6.274	302.1	0.005
1.8	5	295	6.176	286.4	0.006
2.5	5	299	5.580	232.1	0.008
3.0	5	297	5.232	182.1	0.006
4.0	5	297	4.677	101.0	0.018
0.5	5	371	3.961	81.5	-0.001
1.1	5	371	5.692	386.9	0.006
1.7	5	372	5.177	414.9	0.004
1.8	5	372	5.099	392.3	0.004
3.0	5	371	4.353	274.1	0.000
4.0	5	372	3.913	155.3	0.011
0.5	5	444	3.478	133.7	-0.001
0.8	5	443	4.473	352.8	0.004
1.1	5	443	4.906	497.6	0.006
1.7	5	444	4.487	548.3	0.004
1.8	5	443	4.422	519.2	0.004
2.5	5	443	4.030	450.6	0.005
3.0	5	444	3.800	398.6	0.006
3.5	5	443	3.604	318.7	0.007
4.0	5	443	3.433	257.3	0.007
0.5	10	295	4.729	20.7	-0.004
1.5	10	298	6.486	285.2	0.002
1.7	10	295	6.277	273.6	0.002
1.8	10	295	6.178	269.0	0.003
1.9	10	295	6.083	271.4	0.004
2.5	10	296	5.580	201.6	0.004
3.0	10	298	5.233	161.5	0.006
4.0	10	298	4.677	75.9	0.026

Table A 3 Experimental data for atmospheric 50:50 H_2:CO at 298 K.

ϕ	P_i (atm)	T_u (K)	σ	$S^0_{L,u}$ (cm/s)	L_m (cm)
0.5	1	296	5.236	31.0	-0.009
0.8	1	297	6.539	82.2	0.003
1.0	1	296	6.911	114.1	0.010
1.2	1	295	6.951	137.1	0.009
1.5	1	296	6.697	166.7	0.010
1.7	1	296	6.495	178.3	0.007
1.8	1	296	6.396	182.1	0.009
1.9	1	297	6.301	180.1	0.008
2.0	1	295	6.209	188.7	0.009
2.5	1	296	5.793	176.2	0.011
3.0	1	295	5.440	154.7	0.013
3.5	1	297	5.138	131.8	0.018
4.0	1	295	4.876	105.9	0.022

Table A 4 Experimental data for 5- and 10-atm 50:50 H_2:CO at 298 K.

ϕ	P_i (atm)	T_u (K)	σ	$S^0_{L,u}$ (cm/s)	L_m (cm)
0.8	5	297	6.466	85.5	0.005
1.0	5	296	7.046	130.5	0.018
1.1	5	297	7.083	140.3	0.008
1.7	5	295	6.392	180.4	0.003
1.9	5	296	6.184	177.0	0.004
2.5	5	296	5.657	144.5	0.005
3.0	5	294	5.302	118.9	0.008
4.0	5	297	4.747	60.2	0.028
0.7	10	295	6.024	45.1	0.004
1.5	10	298	6.625	169.0	0.005
1.8	10	295	6.288	172.2	0.004
2.0	10	298	6.088	163.7	0.003
3.0	10	294	5.302	89.1	0.004

Table A 5 Experimental data for Exps. 1, 2, and 3 in Table 7.

H_2	CO	H_2O (% by mole)	ϕ	P_i (atm)	T_u (K)	σ	$S^0_{L,u}$ (cm/s)	$L_{m,u}$ (cm)	Absolute U_{SL} (cm/s)
5	95	7.5	0.60	1	320	5.452	21.6	0.008	4.2
5	95	7.5	0.60	1	321	5.452	21.7	0.009	4.2
5	95	7.5	0.60	1	323	5.452	22.4	0.011	4.2
5	95	7.5	0.70	1	325	5.828	29.5	0.009	4.2
5	95	7.5	0.80	1	325	6.101	36.1	0.010	4.2
5	95	7.5	0.90	1	325	6.279	42.1	0.012	4.2
5	95	7.5	1.00	1	322	6.383	47.8	0.010	4.2
5	95	7.5	1.30	1	322	6.406	62.3	0.011	4.2
5	95	7.5	1.70	1	323	6.085	74.2	0.009	4.2
5	95	7.5	1.80	1	322	5.994	76.5	0.008	4.2
5	95	7.5	1.80	1	322	5.994	77.6	0.009	4.2
5	95	7.5	2.00	1	322	5.818	78.5	0.005	4.2
5	95	7.5	2.30	1	325	5.575	82.2	0.008	4.2
5	95	7.5	2.50	1	323	5.426	82.9	0.009	4.2
5	95	7.5	2.70	1	325	5.287	81.0	0.005	4.2
5	95	7.5	3.00	1	323	5.096	76.7	0.007	4.2
5	95	7.5	3.50	1	322	4.816	64.3	0.013	4.2
5	95	7.5	4.00	1	322	4.577	55.9	0.012	4.2
5	95	7.5	5.00	1	322	4.188	28.8	0.017	4.4
50	50	0.0	0.55	5	323	4.890	40.5	0.008	4.2
50	50	0.0	0.95	5	323	6.463	129.5	0.006	4.2
50	50	0.0	1.20	5	322	6.506	164.6	0.004	4.2
50	50	0.0	1.25	5	322	6.452	176.7	0.004	4.2
50	50	0.0	1.50	5	323	6.169	199.4	0.004	4.2
50	50	0.0	1.65	5	322	6.010	205.5	0.003	4.2
50	50	0.0	1.80	5	322	5.861	201.9	0.004	4.2
50	50	0.0	1.80	5	325	5.861	204.7	0.003	4.2
50	50	0.0	1.85	5	322	5.813	210.2	0.004	4.2
50	50	0.0	2.30	5	322	5.430	201.1	0.005	4.3
50	50	0.0	2.80	5	323	5.078	151.9	0.004	4.9
50	50	0.0	3.30	5	323	4.784	119.7	0.005	6.0
50	50	0.0	3.80	5	323	4.533	88.1	0.009	7.6
50	50	0.0	4.80	5	323	4.127	34.8	0.074	8.0
100	0	15	0.45	1	322	4.343	56.1	-0.005	4.2
100	0	15	0.45	1	325	4.343	55.1	-0.009	4.2
100	0	15	0.65	1	323	5.235	117.0	-0.006	4.2
100	0	15	1.05	1	322	6.203	231.1	0.009	4.2
100	0	15	1.05	1	325	6.203	229.3	0.007	4.2
100	0	15	1.35	1	322	5.941	274.2	0.008	4.2
100	0	15	1.35	1	325	5.941	266.9	0.005	4.2
100	0	15	1.75	1	324	5.554	281.6	0.010	4.2
100	0	15	1.90	1	322	5.421	270.3	0.009	4.2
100	0	15	1.90	1	325	5.421	273.8	0.010	4.2
100	0	15	2.10	1	324	5.255	260.3	0.010	4.2
100	0	15	2.60	1	325	4.886	223.4	0.013	4.2
100	0	15	3.10	1	325	4.574	185.2	0.018	4.3
100	0	15	3.60	1	325	4.307	147.7	0.023	4.4

Table A 6 Experimental data for Exps. 4, 5, and 6 in Table 7.

H_2	CO	H_2O (% by mole)	ϕ	P_i (atm)	T_u (K)	σ	$S^0_{L,u}$ (cm/s)	$L_{m,u}$ (cm)	Absolute U_{SL} (cm/s)
100	0	0.0	0.50	1	370	4.180	95.3	-0.010	4.2
100	0	0.0	0.70	1	373	4.938	187.8	0.000	4.2
100	0	0.0	0.90	1	373	5.459	264.8	0.005	4.2
100	0	0.0	1.10	1	373	5.635	325.3	0.008	4.2
100	0	0.0	1.30	1	372	5.524	357.8	0.007	4.2
100	0	0.0	1.70	1	370	5.237	383.5	0.009	4.2
100	0	0.0	1.90	1	371	5.099	382.8	0.012	4.2
100	0	0.0	2.50	1	374	4.725	349.3	0.014	4.2
100	0	0.0	3.00	1	372	4.456	310.3	0.015	4.3
100	0	0.0	3.50	1	373	4.220	273.9	0.020	4.5
100	0	0.0	4.00	1	372	4.013	234.8	0.020	4.9
100	0	0.0	4.50	1	373	3.831	204.7	0.025	5.3
100	0	0.0	5.00	1	373	3.668	174.9	0.032	5.4
5	95	15	0.65	5	373	4.582	36.9	0.027	4.2
5	95	15	0.90	5	374	5.494	60.4	0.012	4.2
5	95	15	1.15	5	373	5.646	75.6	0.008	4.2
5	95	15	1.45	5	374	5.377	86.5	0.006	4.2
5	95	15	1.80	5	373	5.058	94.5	0.005	4.2
5	95	15	2.00	5	373	4.898	93.3	0.005	4.2
5	95	15	2.40	5	373	4.618	83.9	0.006	4.2
5	95	15	2.90	5	373	4.329	66.4	0.005	4.5
5	95	15	3.30	5	373	4.135	54.9	0.005	4.9
5	95	15	3.80	5	373	3.930	34.0	0.016	5.8
5	95	15	4.20	5	373	3.789	25.1	0.029	6.6
50	50	7.5	0.60	10	373	4.512	46.4	0.003	4.2
50	50	7.5	0.80	10	373	5.241	99.8	0.004	4.2
50	50	7.5	1.00	10	372	5.692	148.7	0.004	4.2
50	50	7.5	1.90	10	373	4.958	197.8	0.004	4.2
50	50	7.5	2.10	10	373	4.805	185.6	0.003	4.5
50	50	7.5	2.40	10	374	4.600	168.1	0.003	4.9
50	50	7.5	2.40	10	373	4.600	169.3	0.002	4.9
50	50	7.5	2.40	10	373	4.600	170.5	0.002	4.9
50	50	7.5	2.40	10	373	4.600	168.8	0.002	4.9
50	50	7.5	2.40	10	373	4.600	170.6	0.003	4.9
50	50	7.5	2.90	10	374	4.310	114.6	0.006	5.8
50	50	7.5	3.40	10	373	4.069	80.4	0.004	7.3

Table A 7 Experimental data for Exps. 7, 8, and 9 in Table 7.

H_2	CO	H_2O (% by mole)	ϕ	P_i (atm)	T_u (K)	σ	$S^0_{L,u}$ (cm/s)	$L_{m,u}$ (cm)	Absolute U_{SL} (cm/s)
50	50	15	0.60	1	424	4.146	84.7	-0.003	4.2
50	50	15	0.75	1	424	4.533	124.0	0.003	4.2
50	50	15	0.95	1	423	4.825	170.6	0.007	4.2
50	50	15	0.95	1	422	4.825	169.2	0.006	4.2
50	50	15	0.95	1	423	4.825	168.5	0.007	4.2
50	50	15	0.95	1	423	4.825	166.5	0.005	4.2
50	50	15	0.95	1	423	4.825	166.4	0.005	4.2
50	50	15	1.15	1	423	4.882	204.4	0.006	4.2
50	50	15	1.35	1	423	4.778	235.8	0.006	4.2
50	50	15	1.65	1	423	4.556	262.5	0.010	4.2
50	50	15	1.90	1	423	4.381	271.4	0.008	4.2
50	50	15	2.10	1	423	4.253	267.1	0.005	4.2
50	50	15	2.60	1	423	3.974	250.5	0.009	4.2
50	50	15	3.10	1	423	3.743	215.7	0.012	4.2
50	50	15	3.60	1	423	3.549	178.1	0.016	4.5
50	50	15	4.10	1	423	3.384	141.2	0.021	5.0
50	50	15	4.50	1	423	3.269	111.5	0.028	5.5
50	50	15	5.00	1	423	3.142	81.2	0.050	5.4
100	0	7.5	0.60	5	423	3.937	181.1	0.000	4.4
100	0	7.5	0.80	5	423	4.569	306.9	0.001	4.4
100	0	7.5	1.10	5	423	5.000	427.1	0.004	4.4
100	0	7.5	1.30	5	423	4.838	461.6	0.002	4.3
100	0	7.5	1.30	5	423	4.838	469.7	0.003	4.3
100	0	7.5	1.80	5	423	4.459	467.2	0.004	4.3
100	0	7.5	2.00	5	423	4.327	455.3	0.004	4.9
100	0	7.5	2.50	5	423	4.037	396.6	0.006	6.0
100	0	7.5	3.00	5	423	3.795	313.9	0.006	7.9
100	0	7.5	3.50	5	423	3.590	258.9	0.010	10.7
100	0	7.5	4.00	5	423	3.413	162.8	0.012	13.9
100	0	7.5	4.00	5	422	3.413	153.7	0.010	13.9
100	0	7.5	4.30	5	423	3.318	154.4	0.014	15.8
100	0	7.5	4.50	5	422	3.259	134.3	0.017	16.7
100	0	7.5	4.50	5	423	3.259	133.4	0.019	16.7
5	95	0	0.60	10	424	4.258	28.7	0.026	4.2
5	95	0	0.85	10	423	5.014	53.2	0.008	4.2
5	95	0	1.05	10	422	5.265	70.3	0.006	4.2
5	95	0	1.25	10	423	5.243	82.2	0.007	4.2
5	95	0	1.60	10	423	4.979	96.2	0.006	4.2
5	95	0	1.90	10	422	4.754	99.0	0.004	4.2
5	95	0	2.10	10	423	4.618	105.4	0.003	4.2
5	95	0	2.60	10	423	4.318	92.8	-0.003	4.2
5	95	0	3.10	10	423	4.067	76.9	0.008	4.3
5	95	0	3.60	10	422	3.853	62.5	0.006	4.7
5	95	0	4.10	10	422	3.669	50.0	0.010	5.6
5	95	0	4.60	10	423	3.509	33.5	0.011	6.5
5	95	0	5.00	10	422	3.395	9.5	0.009	5.4

NUIG Mechanism

Themodynamics

```
!Authors:A.K. Keromnes, W. K. Metcalfe, H. J. Curran
thermo
300.000  1000.000  5000.000
h               l 6/94h   1    0    0    0g   200.000  6000.00  1000.00      1
0.25000000e+01 0.00000000e+00 0.00000000e+00 0.00000000e+00 0.00000000e+00    2
0.25473660e+05-0.44668285e+00 0.25000000e+01 0.00000000e+00 0.00000000e+00    3
0.00000000e+00 0.00000000e+00 0.25473660e+05-0.44668285e+00 0.26219035e+05    4
h2              tpis78h   2    0    0    0g   200.000  6000.00  1000.00      1
2.93286575e+00 8.26608026e-04-1.46402364e-07 1.54100414e-11-6.88804800e-16    2
-8.13065581e+02-1.02432865e+00 2.34433112e+00 7.98052075e-03-1.94781510e-05    3
2.01572094e-08-7.37611761e-12-9.17935173e+02 6.83010238e-01 0.00000000e+00    4
o               l 1/90o   1    0    0    0g   200.000  6000.00  1000.00      1
2.54363697e+00-2.73162486e-05-4.19029520e-09 4.95481845e-12-4.79553694e-16    2
2.92260120e+04 4.92229457e+00 3.16826710e+00-3.27931884e-03 6.64306396e-06    3
-6.12806624e-09 2.11265971e-12 2.91222592e+04 2.05193346e+00 2.99687009e+04    4
o2              rus 89o   2    0    0    0g   200.000  6000.00  1000.00      1
3.66096065e+00 6.56365811e-04-1.41149627e-07 2.05797935e-11-1.29913436e-15    2
-1.21597718e+03 3.41536279e+00 3.78245636e+00-2.99673416e-03 9.84730201e-06    3
-9.68129509e-09 3.24372837e-12-1.06394356e+03 3.65767573e+00 0.00000000e+00    4
oh              iu3/03o   1 h  1    0    0g   200.000  6000.00  1000.00      1
2.83853033e+00 1.10741289e-03-2.94000209e-07 4.20698729e-11-2.42289890e-15    2
3.69780808e+03 5.84494652e+00 3.99198424e+00-2.40106655e-03 4.61664033e-06    3
-3.87916306e-09 1.36319502e-12 3.36889836e+03-1.03998477e-01 4.48613328e+03    4
oh*             121286o   1h   1         g  0300.00   5000.00  1000.00      1
0.02882730e+02 0.10139743e-02-0.02276877e-05 0.02174683e-09-0.05126305e-14    2
5.02650000e+04 0.05595712e+02 0.03637266e+02 0.01850910e-02-0.16761646e-05    3
0.02387202e-07-0.08431442e-11 5.00213000e+04 0.13588605e+01                   4
h2o             l 5/89h   2 o  1    0    0g   200.000  6000.00  1000.00      1
0.26770389e+01 0.29731816e-02-0.77376889e-06 0.94433514e-10-0.42689991e-14    2
-0.29885894e+05 0.68825500e+01 0.41986352e+01-0.20364017e-02 0.65203416e-05    3
-0.54879269e-08 0.17719680e-11-0.30293726e+05-0.84900901e+00-0.29084817e+05    4
n2              g 8/02n   2    0    0    0g   200.000  6000.00  1000.00      1
2.95257637e+00 1.39690040e-03-4.92631603e-07 7.86010195e-11-4.60755204e-15    2
-9.23948688e+02 5.87188762e+00 3.53100528e+00-1.23660988e-04-5.02999433e-07    3
2.43530612e-09-1.40881235e-12-1.04697628e+03 2.96747038e+00 0.00000000e+00    4
ho2             t 1/09h   1o   2    0    0g   200.000  5000.00  1000.00      1
4.17228741e+00 1.88117627e-03-3.46277286e-07 1.94657549e-11 1.76256905e-16    2
3.10206839e+01 2.95767672e+00 4.30179807e+00-4.74912097e-03 2.11582905e-05    3
-2.42763914e-08 9.29225225e-12 2.64018485e+02 3.71666220e+00 1.47886045e+03    4
h2o2            t 8/03h   2o   2    0    0g   200.000  6000.00  1000.00      1
4.57977305e+00 4.05326003e-03-1.29844730e-06 1.98211400e-10-1.13968792e-14    2
-1.80071775e+04 6.64970694e-01 4.31515149e+00-8.47390622e-04 1.76404323e-05    3
-2.26762944e-08 9.08950158e-12-1.77067437e+04 3.27373319e+00-1.63425145e+04    4
ar              g 5/97ar  1  0    0      0g   200.000  6000.00  1000.00      1
2.50000000e+00 0.00000000e+00 0.00000000e+00 0.00000000e+00 0.00000000e+00    2
-7.45375000e+02 4.37967491e+00 2.50000000e+00 0.00000000e+00 0.00000000e+00   3
0.00000000e+00 0.00000000e+00-7.45375000e+02 4.37967491e+00 0.00000000e+00    4
co              rus 79c   1o   1    0    0g   200.000  6000.00  1000.00      1
0.30484859e+01 0.13517281e-02-0.48579405e-06 0.78853644e-10-0.46980746e-14    2
-0.14266117e+05 0.60170977e+01 0.35795335e+01-0.61035369e-03 0.10168143e-05    3
0.90700586e-09-0.90442449e-12-0.14344086e+05 0.35084093e+01-0.13293628e+05    4
co2             l 7/88c   1o   2    0    0g   200.000  6000.00  1000.00      1
0.46365111e+01 0.27414569e-02-0.99589759e-06 0.16038666e-09-0.91619857e-14    2
-0.49024904e+05-0.19348955e+01 0.23568130e+01 0.89841299e-02-0.71220632e-05    3
0.24573008e-08-0.14288548e-12-0.48371971e+05 0.99009035e+01-0.47328105e+05    4
he              g 5/97he 1    0    0    0 g   200.000  6000.00  1000.00      1
2.50000000e+00 0.00000000e+00 0.00000000e+00 0.00000000e+00 0.00000000e+00    2
-7.45375000e+02 9.28723974e-01 2.50000000e+00 0.00000000e+00 0.00000000e+00   3
0.00000000e+00 0.00000000e+00-7.45375000e+02 9.28723974e-01 0.00000000e+00    4
ch4             g 8/99c  1 h  4    0    0 g   200.000  6000.00  1000.00      1
```

1.65326226e+00 1.00263099e-02-3.31661238e-06 5.36483138e-10-3.14696758e-14 2
-1.00095936e+04 9.90506283e+00 5.14911468e+00-1.36622009e-02 4.91453921e-05 3
-4.84246767e-08 1.66603441e-11-1.02465983e+04-4.63848842e+00-8.97226656e+03 4
c2h6 g 8/88c 2h 6 0 0g 200.000 6000.00 1000.00 1
4.04666411e+00 1.53538802e-02-5.47039485e-06 8.77826544e-10-5.23167531e-14 2
-1.24473499e+04-9.68698313e-01 4.29142572e+00-5.50154901e-03 5.99438458e-05 3
-7.08466469e-08 2.68685836e-11-1.15222056e+04 2.66678994e+00-1.00849652e+04 4
hco t 5/03c 1 h 1 o 1 0 g 200.000 6000.00 1000.00 1
3.92001542e+00 2.52279324e-03-6.71004164e-07 1.05615948e-10-7.43798261e-15 2
3.65342928e+03 3.58077056e+00 4.23754610e+00-3.32075257e-03 1.40030264e-05 3
-1.34239995e-08 4.37416208e-12 3.87241185e+03 3.30834869e+00 5.08749163e+03 4
End

Transport

!Authors:A.K. Keromnes, W. K. Metcalfe, H. J. Curran
h 0 145 2.05 0 0 0 !
h2 1 38 2.92 0 0.79 280 !
o 0 80 2.75 0 0 0 !
o2 1 107.4 3.458 0 1.6 3.8 !
oh 1 80 2.75 0 0 0 !
oh* 1 80 2.75 0 0 0 !
h2o 2 572.4 2.605 1.844 0 4 !
n2 1 97.53 3.621 0 1.76 4 !
ho2 2 107.4 3.458 0 0 1 !
h2o2 2 107.4 3.458 0 0 3.8 !
ar 0 136.5 3.33 0 0 0 !
co 1 98.1 3.65 0 1.95 1.8 !
co2 1 244 3.763 0 2.65 2.1 !
he 0 10.2 2.576 0 0 0 !
ch4 2 141.4 3.746 0 2.6 13 !
c2h6 2 247.5 4.35 0 0 1.5 !
hco 2 498 3.59 0 0 0 !

Chemkin Input

!Authors:A.K. Keromnes, W. K. Metcalfe, H. J. Curran
elements
c h n o ar he
end
species
h h2 o o2 oh oh*
h2o n2 ho2 h2o2 ar
co co2 he ch4 c2h6 hco
end
reactions
!ref:3 parameter fit to hong et al.proc. of the comb. inst. 33 (2011) 309–316
h+o2<=>o+oh 9.65e+14 -0.262 1.62e+04
!ref:sutherland et al., 21st symposium, p. 929 (1986)
o+h2<=>h+oh 5.080e+04 2.670 6.292e+03
!ref:! oldenborg,r.c.et al. j. phys. chem. (1992) 96 8426-8430
oh+h2<=>h+h2o 2.247e8 1.520 3.450e+03
!ref:sutherland et al., 23rd symposium, p. 51 (1990) increased by 16% for h2-co-h2o flames
o+h2o<=>oh+oh 3.445e+06 2.020 1.340e+04
!ref:tsang and hampson, j. phys. chem. ref. data, 15:1087 (1986)
h2+m<=>h+h+m 4.577e+19 -1.400 1.044e+05
h2/ 2.5/ h2o/ 12/ co/ 1.9/ co2/ 3.8/ he/ .83/ ch4/ 2/ c2h6/ 3/
o+o+m<=>o2+m 6.165e+15 -0.500 0.000e+00
h2/ 2.5/ h2o/ 12/ ar/ .83/ co/ 1.9/ co2/ 3.8/ he/ .83/ ch4/ 2/ c2h6/ 3/
o+h+m<=>oh+m 4.714e+18 -1.000 0.000e+00
h2/ 2.5/ h2o/ 12/ ar/ .75/ co/ 1.5/ co2/ 2/ he/ .75/ ch4/ 2/ c2h6/ 3/
!ref: li ijck 36: 566–575, 2004
!ref:optimised to fit H2 and CH4 flames data
h+oh+m<=>h2o+m 3.5e+22 -2.000 0.000e+00

```
h2/ 2.5/ h2o/ 12/ ar/ 0.38/ he/ 0.38/ co/ 1.9/ co2/ 3.8/ ch4/ 2/ c2h6/ 3/
!ref:fernandes pccp 2008
h+o2(+m)<=>ho2(+m) 4.650e+12 0.440 0.000e+00
low/ 1.737e+19 -1.23 0.000e+00/
troe/ 0.67 1e-30 1e30 1e30/
h2/ 1.3/ co/ 1.9/ co2/ 3.8/ he/ 0.0/ h2o/ 10.0/ ar/ 0.00/ ch4/ 2/ c2h6/ 3/
h+o2(+ar)<=>ho2(+ar) 4.650e+12 0.440 0.000e+00
!ref: bates et al. pccp 3 (2001) 2337-2342
low/ 6.810e+18 -1.200 0.0/
troe/ 0.70 1.0e-30 1.0e+30 1.0e+30/
!ref:LPL * 1.5 AK
h+o2(+he)<=>ho2(+he) 4.650e+12 0.440 0.000e+00
low/ 9.192e+18 -1.20 0.000e+00/
troe/ 0.59 1e-30 1e30 1e30/
!ref: mueller 99
ho2+h<=>oh+oh 7.079e+13 0.00 2.950e+02
!ref:michael sutherland 2000
h2+o2<=>h+ho2 5.176e+05 2.433 53502.0
!ref:baulch et al., j. phys. chem. ref data, 21:411 (1992)
ho2+o<=>oh+o2 3.250e+13 0.000 0.000e+00
!ref:keyser, j. phys. chem. 92:1193 (1988) reduced by 15%
ho2+oh<=>h2o+o2 2.456e+13 0.000 -4.970e+02
!ref:Hippler et al. j.chem.phys 93 1755-1760 (1990)
ho2+ho2<=>h2o2+o2 1.300e+11 0.000 -1630.00
dup
!ref:reduced by 13%
ho2+ho2<=>h2o2+o2 3.658e+14 0.000 12000.00
dup
!ref:troe, combust. flame, 158:594-601 (2011)
!ref:rate constant is for n2
h2o2(+h2o)<=>oh+oh(+h2o) 2.00e+12 0.90 4.8749+04
low/ 1.865e+25 -2.30 4.8749+04/
troe/ 0.51 1e-30 1e+30/
h2o2(+m)<=>oh+oh(+m) 2.00e+12 0.90 4.8749+04
low/ 2.49e+24 -2.30 4.8749+04/
troe/ 0.43 1e-30 1e+30/
h2o/ 0.0/ co2/ 1.6/ n2/ 1.5/ o2/ 1.2/ he/ 0.65/ h2o2/ 7.7/
!ref:efficiencies for h2 and co taken from li et al., int. j. chem. kinet. 36:566-575 (2004)
h2/ 3.7/ co/ 2.8/
!ref:tsang and hampson, j. phys. chem. ref. data, 15:1087 (1986)
h2o2+h<=>h2o+oh 2.410e+13 0.000 3.970e+03
!ref: ellingson j. phys. chem. (2007) 111, (51), 13554-13566
h2o2+h<=>h2+ho2 2.150e+10 1.000 6.000e+03
!ref:tsang and hampson, j. phys. chem. ref. data, 15:1087 (1986)
h2o2+o<=>oh+ho2 9.550e+06 2.000 3.970e+03
!ref: hong et al. j. phys. chem. a 114 (2010) 5718-5727
h2o2+oh<=>h2o+ho2 1.74e+12 0.000 3.18e+02
dup
h2o2+oh<=>h2o+ho2 7.59e+13 0.000 7.269e+03
dup
!ref:meuller 99 * 0.76
co+o(+m)<=>co2(+m) 1.362e+10 0.000 2384.00
low/ 1.173e+24 -2.79 4191.0/
h2/ 2.0/ h2o/ 12/ co/ 1.75/ co2/ 3.6/ ar/ 0.7/ he/ 0.7/
!ref:86tsa/ ham * 0.44
co+o2<=>co2+o 1.119e+12 0.000 47700.00
!ref: joshi and wang ijck (2006), 38, (1), 57-73.
co+oh<=>co2+h 7.015e+04 2.053 -355.67
dup
co+oh<=>co2+h 5.757e+12 -0.664 331.83
dup
!ref:you et al. j. phys. chem. a 2007, 111, 4031-4042
co+ho2<=>co2+oh 1.570e+05 2.180 1.794e+04
!ref:li et al. ijck 2007
hco+m<=>h+co+m 4.750e+11 0.660 1.487e+04
h2/ 2/ h2o/ 12/ co/ 1.5/ co2/ 2/ ch4/ 2/ c2h6/ 3/
```

```
!ref:timonen et al., jpc, 92:651 (1988)
hco+o2<=>co+ho2 7.580e+12 0.000 4.100e+02
hco+h<=>co+h2 7.340e+13 0.000 0.000e+00
!ref:tsang and hampson, j. phys. chem. ref. data, 15:1087 (1986)
hco+o<=>co+oh 3.020e+13 0.000 0.000e+00
hco+o<=>co2+h 3.000e+13 0.000 0.000e+00
!ref:timonen et al., jpc, 92:651 (1988)
hco+oh<=>co+h2o 1.020e+14 0.000 0.000e+00
!ref:tsang and hampson, j. phys. chem. ref. data, 15:1087 (1986)
hco+ho2=>co2+h+oh 3.000e+13 0.000 0.000e+00
!ref:tsang and hampson, j. phys. chem. ref. data, 15:1087 (1986)
hco+hco=>h2+co+co 3.000e+12 0.000 0.000e+00
!ref:oh* ************************************************** kathrotia et al. comb & flame 2010
h+o+m<=>m+oh* 1.50e+13 0.0 5.975e3
h2/ 1/ h2o/ 6.5/ o2/ 0.4/ n2/ 0.4/ ar/ 0.35/
oh*+h2o<=>oh+h2o 5.930e+12 0.5 -8.60e2
oh*+h2<=>oh+h2 2.950e+12 0.5 -4.44e2
oh*+n2<=>oh+n2 1.080e+11 0.5 -1.242e3
oh*+oh<=>oh+oh 6.010e+12 0.5 -7.64e2
oh*+h<=>oh+h 1.310e+12 0.5 -1.67e2
oh*+ar<=>oh+ar 1.690e+12 0.0 4.135e3
oh*<=>oh+hv 1.450e+06 0.0 0.0
oh*+o2<=>oh+o2 2.100e+12 0.5 -4.78e2
oh*+co2<=>oh+co2 2.750e+12 0.5 -9.68e2
oh*+co<=>oh+co 3.230e+12 0.5 -7.87e2
oh*+ch4<=>oh+ch4 3.360e+12 0.5 -6.35e2
end
```

Premix Sample

```
!Note:Due to limitations in Chemkin with respect to the treatment of third body reactions in the form:
!     A+B(+X)=AB(+X), where X=Ar, He, H2O etc... it is necessary to include small concentrations of X to avoid
!     convergence issues. The example below is a robust an efficient example of a Premix input file for use with
!     the mechanism prsented in this publication.
!
! problem type definition
!
ENRG   ! Solve Gas Energy Equation
FREE   ! Freely Propagating Flame
MULT   ! Use Multicomponent Transport
VCOR   ! Use Correction Velocity Formalism
TDIF
!
! physical property
!
FLRT 0.06   ! Mass Flow Rate (g/cm2-sec)
PRES 5.0   ! Pressure (atm)
TUNBURNT 323.0   ! Unburnt Gas Temperature (K)
!
! reactor dimension definition
!
CURV 0.99   ! Adaptive Grid Control Based On Solution Curvature
GRAD 0.99   ! Adaptive Grid Control Based On Solution Gradient
NADP 50   ! Number of Adaptive Grid Points
NTOT 3000   ! Maximum Number of Grid Points Allowed
XEND 0.3   ! Ending Axial Position (cm)
XSTR 0.0   ! Starting Axial Position (cm)
!
! species property
!
INTM h 0.02   ! Intermediate Fraction (mole fraction)
INTM h2 0.01   ! Intermediate Fraction (mole fraction)
INTM h2o2 0.0001   ! Intermediate Fraction (mole fraction)
```

```
INTM hco 1.0E-5   ! Intermediate Fraction (mole fraction)
INTM ho2 0.0001   ! Intermediate Fraction (mole fraction)
INTM o 0.0001   ! Intermediate Fraction (mole fraction)
INTM oh 0.001   ! Intermediate Fraction (mole fraction)
MOLE   ! Print Mole Fractions
PRMN 0.0   ! Minimum for Product Estimates (mole fraction)
REAC h2 0.50000
REAC co 0.50000
REAC o2 0.50000
REAC h2o 0.00000
REAC he 3.50000

!Added to prevent convergence issues in CKPro 15101 due to h2o2(+co2) reaction
REAC h2o 2e-2

!Added to prevent convergence issues in CKPro 15101 due to h+o2(+ar) reaction
REAC ar 1e-10

XIMN 0.0   ! Minimum for Estimated Intermediate Fraction (mole fraction)
!
! solver control
!
ATIM 1.0E-5   ! Absolute Tolerance for Pseudo Timestepping
ATOL 1.0E-9   ! Absolute Tolerance
IRET 200   ! Number Time Steps Before Increasing
RTIM 1.0E-5   ! Relative Tolerance for Pseudo Timestepping
RTOL 0.0001   ! Relative Tolerance
SFLR -0.001   ! Minimum Bounds on Species Fractions
SPOS 1.0e-8   ! Positive Value to Reset Species Fractions
TIM1 100.0 5.0E-7   ! Pseudo Time Steps (Fixed Temperature) (none, sec)
TIM2 200.0 1.0E-6   ! Pseudo Time Steps (Energy Equation) (none, sec)
TPROF   ! Automatic Estimated Temperature Profile
USE_TPRO_GRID   ! Based On Temperature Profile Estimate
WDIF   ! Windward Differencing
!
! output control and other misc. property
!
GFAC 1.0   ! Gas Reaction Rate Multiplier
PRNT 1   ! Print Level Control
! Number of Continuation 10   ! Continuation Count
CNTN   ! Continuation
END   ! End
CURV 0.9   ! Adaptive Grid Control Based On Solution Curvature
GRAD 0.9   ! Adaptive Grid Control Based On Solution Gradient
XEND 8.0   ! Ending Axial Position (cm)
XSTR -0.5   ! Starting Axial Position (cm)
CNTN   ! Continuation
END   ! End
CURV 0.8   ! Adaptive Grid Control Based On Solution Curvature
GRAD 0.8   ! Adaptive Grid Control Based On Solution Gradient
XEND 8.0   ! Ending Axial Position (cm)
XSTR -0.5   ! Starting Axial Position (cm)
CNTN   ! Continuation
END   ! End
CURV 0.7   ! Adaptive Grid Control Based On Solution Curvature
GRAD 0.7   ! Adaptive Grid Control Based On Solution Gradient
XEND 8.0   ! Ending Axial Position (cm)
XSTR -0.5   ! Starting Axial Position (cm)
CNTN   ! Continuation
END   ! End
CURV 0.5   ! Adaptive Grid Control Based On Solution Curvature
GRAD 0.5   ! Adaptive Grid Control Based On Solution Gradient
XEND 10.0   ! Ending Axial Position (cm)
XSTR -1.0   ! Starting Axial Position (cm)
CNTN   ! Continuation
END   ! End
```

```
CURV 0.25   ! Adaptive Grid Control Based On Solution Curvature
GRAD 0.25   ! Adaptive Grid Control Based On Solution Gradient
CNTN   ! Continuation
END   ! End
CURV 0.25   ! Adaptive Grid Control Based On Solution Curvature
GRAD 0.25   ! Adaptive Grid Control Based On Solution Gradient
XSTR -2.0   ! Starting Axial Position (cm)
CNTN   ! Continuation
END   ! End
CURV 0.1   ! Adaptive Grid Control Based On Solution Curvature
GRAD 0.2   ! Adaptive Grid Control Based On Solution Gradient
XSTR -4.0   ! Starting Axial Position (cm)
CNTN   ! Continuation
END   ! End
TDIF   ! Use Thermal Diffusion (Soret Effect)
VCOR   ! Use Correction Velocity Formalism
CURV 0.1   ! Adaptive Grid Control Based On Solution Curvature
GRAD 0.1   ! Adaptive Grid Control Based On Solution Gradient
XSTR -10.0   ! Starting Axial Position (cm)
CNTN   ! Continuation
END   ! End
REAC h2 0.50000
REAC co 0.50000
REAC o2 0.50000
REAC h2o 0.00000
REAC he 3.50000

!Added to prevent convergence issues in CKPro 15101 due to h2o2(+h2o) reaction
REAC h2o 1e-10

!Added to prevent convergence issues in CKPro 15101 due to h+o2(+ar) reaction
REAC ar 1e-10
TDIF   ! Use Thermal Diffusion (Soret Effect)
VCOR   ! Use Correction Velocity Formalism
CURV 0.02   ! Adaptive Grid Control Based On Solution Curvature
GRAD 0.02   ! Adaptive Grid Control Based On Solution Gradient
XEND 20.0   ! Ending Axial Position (cm)
CNTN   ! Continuation
END   ! End
TDIF   ! Use Thermal Diffusion (Soret Effect)
VCOR   ! Use Correction Velocity Formalism
CURV 0.01   ! Adaptive Grid Control Based On Solution Curvature
GRAD 0.01   ! Adaptive Grid Control Based On Solution Gradient
XEND 100.0   ! Ending Axial Position (cm)
XSTR -20.0   ! Starting Axial Position (cm)
END
```

VITA

Michael Christopher Krejci received his Bachelor of Science degree in mechanical engineering from Texas A&M University in 2010. He then entered the graduate program at Texas A&M University and received his Master of Science degree in mechanical engineering in May of 2012. During his graduate work, Krejci authored 2 journal publications and 2 conference papers. He also gave presentations at 2 national conferences. His interests include experimental design, experimental testing, and gas dynamics.

Mr. Krejci may be reached at the Department of Mechanical Engineering, 3123 TAMU, Texas A&M University, College Station, TX 77843-3123. His email is mck1887@tamu.edu